

7-15-2010

# Synthesis and Characterization of Zinc Oxide Complex Nanostructures

Dinghao Tang

*University of Missouri-St. Louis*, dtang@umsl.edu

Follow this and additional works at: <http://irl.umsl.edu/thesis>

---

## Recommended Citation

Tang, Dinghao, "Synthesis and Characterization of Zinc Oxide Complex Nanostructures" (2010). *Theses*. 278.  
<http://irl.umsl.edu/thesis/278>

This Thesis is brought to you for free and open access by the Graduate Works at IRL @ UMSL. It has been accepted for inclusion in Theses by an authorized administrator of IRL @ UMSL. For more information, please contact [marvinh@umsl.edu](mailto:marvinh@umsl.edu).

SYNTHESIS AND CHARACTERIZATION OF ZINC OXIDE COMPLEX NANOSTRUCTURES

by

DINGHAO TANG

A THESIS

Presented to the Academic Faculty and the Graduate School of the

UNIVERSITY OF MISSOURI - ST. LOUIS

In Partial Fulfillment of the Requirements for the Degree

MASTER OF SCIENCE

in the

Department of Physics & Astronomy, College of Science & Arts

University of Missouri - St. Louis

Advisory Committee:

Jingyue Liu, Ph.D.

*Chairperson of Advisory Committee*

Philip Fraundorf, Ph.D.

*Director of Graduate Program*

Eric Majzoub, Ph.D.

Date Finished: August 5th, 2010

DINGHAO TANG

All Rights Reserved

University of Missouri - St. Louis

August, 2010

## **ABSTRACT**

Zinc Oxide nanostructures are important for many applications, specifically for developing novel catalysts and sensors which our research group has been working on. The objectives of this thesis are: (1) synthesis and characterization of complex ZnO nanostructures; (2) development of synthesis protocols for high-yield and reliable synthesis of nanostructures.

In this thesis, chapter 1 introduces the background of nanoscience and nanotechnology, with a focus on nanomaterials. In chapter 2, the fundamental knowledge of ZnO and relevant characterization techniques are introduced, specifically the crystallography of ZnO wurtzite structure and the scanning (translation) electron microscopy. Several goals have been achieved and they are reported in chapter 3 and 4. First, the nano-pyramid decorated microwires were fabricated. A growth mechanism for those complex nanostructures was proposed. Second, surface modification such as grooved surfaces of ZnO nanostructures has been realized. Grooved nanowires, microbelts, and micrometer-scale tetra-pods are discussed. Third, the effects of oxygen partial pressure on the growth of ZnO have been investigated.

All the ZnO nanostructures reported in this thesis were synthesized by a physical vapor deposition method. The field-emission scanning electron microscope was used to examine the morphologies of the synthesized nanostructures. Aberration-corrected scanning transmission electron microscopy provided information on fabricated nanostructures.

## ACKNOWLEDGMENTS

I would like to express my deepest love, respect, and admiration to my parents for their unconditional care, support, and understanding in every possible way in those years.

In regards to faculty at University of Missouri-St. Louis (UMSL), I would like to extend my greatest appreciation to my mentors that have helped define my path of travel. More specifically, to Dr. Jingyue (Jimmy) Liu for his inspiration, advice and guidance on the research projects and most demanding of circumstances; to Dr. Dan Zhou, Dr. David Osborn and Mr. Wayne Garver, for the instruments' training and technical supports; to Dr. Philip Fraundorf, Dr. Eric Majzoub and Dr. Jingyue Liu for serving as my advisory committee members.

In regards to institutes at UMSL, I would like to acknowledge Department of Physics & Astronomy for the opportunities and financial support for my Master studies. I would like to thank the Center for Nanoscience for providing facilities for my research.

In regards to the my projects' collaborations, I would like to thank the staff members, specially to Dr. Lawrence Allard and et al, at Advanced Microscopy Laboratory in Materials Science and Technology Division at Oak Ridge National Laboratory, for the remarkable opportunities of accessing the facilities and learning the techniques.

Finally, I would like to thank the funds provided by University of Missouri-St. Louis and various external funding elsewhere, to support my research projects.

## TABLE OF CONTENTS

ABSTRACT.....	i
ACKNOWLEDGMENTS.....	ii
Chapter 1. Introduction .....	1
1.1. The nanoscience and nanotechnology—from "top-down" to "bottom-up" .....	1
1.2. Nanomaterials.....	2
1.3. One dimensional nanostructures.....	3
1.4. One-dimensional ZnO structures .....	4
1.4.1. Synthesis of 1-D ZnO nanostructures .....	4
1.4. Goals of the thesis.....	9
Chapter 2. Fundamentals of Zinc Oxide.....	10
2.1. Introduction to crystallography .....	10
2.2. Expressions of lattice directions and crystal planes for ZnO wurtzite structure ...	10
2.2.1. Miller-Bravais 4-D coordinates for lattice directions and crystal planes of ZnO wurtzite structure .....	10
2.2.1. Conversions of lattice directions and crystal planes between 3-D coordinate and 4-D coordinate .....	11
2.2. Basic crystallography of Zinc Oxide.....	13
2.3. Characterization techniques .....	16
2.3.1. Electron Microscopy .....	17
2.4. General understanding of ZnO 1-D nanostructures .....	19
2.5. Ideal candidate of 1D nanostructure for surface functionalization.....	20
2.6. Kinematical SADP electron diffraction simulation .....	22
Chapter 3: Synthesis and Characterization of 1D Complex ZnO Nanostructures.....	25
3.1. Synthesis and Characterization of Nano-pyramid Decorated ZnO Microwires.....	25
3.1.1. Synthesis of nano-pyramid decorated ZnO microwires .....	25
3.1.2. Characterization of nano-pyramid decorated ZnO microwires .....	26
3.1.3. Possible growth mechanism of nano-pyramid decorated microwires .....	36
3.2. Spontaneous surface ordering of ZnO Nanostructures by Physical Vapor Deposition.....	38

3.2.1. Synthesis of grooved surface ZnO nanowires.....	38
3.2.2. Characterization of grooved surface ZnO nanowires .....	38
3.2.3. Thermodynamic model for the periodic distance's dependence on nanowires' diameters .....	41
3.2.4. Growth mechanism of grooved surface nanowires.....	43
3.2.5. Characterization of other surface grooved patterns .....	44
Chapter 4: The Effects of Oxygen Partial Pressure on the Morphologies of ZnO Nanostructures and their high yield synthesis .....	49
4.1. High-yield synthesis of characterization of several typical nanomaterials due to the effect of oxygen partial pressure.....	49
4.1.1. Zn microparticles .....	50
4.1.2. Grey gel-like nanomaterials .....	53
4.1.3. White gel-like ZnO nanomaterials .....	55
4.2. Reasons for large amount of as-grown products.....	57
APPENDIX: PUBLICATIONS .....	59
VITA.....	60
REFERENCES.....	61

## Chapter 1. Introduction

### 1.1. The nanoscience and nanotechnology—from "top-down" to "bottom-up"

The modern technologies rely on electron-operated devices and circuits, especially for the integrated circuits (ICs). The fabrication processes of modern ICs are based on a top-down strategy—breaking down large pieces of semiconductors into nanometer-scale components and integrating these components into a functional device. The top-down approach begins from bulk materials, which is then sculpted into nanometer scale features by carving, milling, etching and patterning. During these processes, lithography techniques are typically used for fabricating integrated circuits. For the development of microelectronics, Moore's Law<sup>1</sup> predicted that the circuit performance doubles and the price down to a half every 18 months. Moore's Law precisely describes a driving force of technological and social change in the late 20th and early 21st centuries. This trend has continued for more than half a century and is not expected to stop until 2015 or latter<sup>2</sup>. Nowadays, current semiconductor technology can fabricate a single transistor with a size below 10 nanometers, almost the size limit for electrical isolation. So what will be the next generation of technology after the period governed by the Moore's Law?

Generally, further shrinking device size through another new technology, or concept, is widely accepted as the answer. The concept of science and technology at the nanometer scale, Nanoscience & Nanotechnology, was introduced firstly by the Nobel Prize winner Dr. Richard Feynman when he gave a talk "There's Plenty of Room at the Bottom" at California Institute of Technology on December 29th, 1959<sup>3</sup>. He proposed the possibility to manipulate individual atoms or molecules by using a set of extremely precise tools, to assemble them into larger structure, device or system with unique properties and functions. This strategy was named as "Bottom up", which was carried

out since the invention of Scanning Tunneling Microscope (STM). A famous example of this approach is that, in 1989, IBM scientists moved atoms with a scanning tunneling microscope. One of the first images seen by the public was of the letters of IBM spelled with xenon atoms on a nickel surface. In the past two decades, plentiful studies with the idea of bottom-up approach were performed, which inspired various novel inventions in the field of Nanoscience and Nanotechnology. Up to the present, the bottom-up approach can be summarized that constructing structures, devices or even systems, from the basic building blocks, such as atoms and molecules. Nanostructures have been playing an important role as building blocks for current cutting-edge research

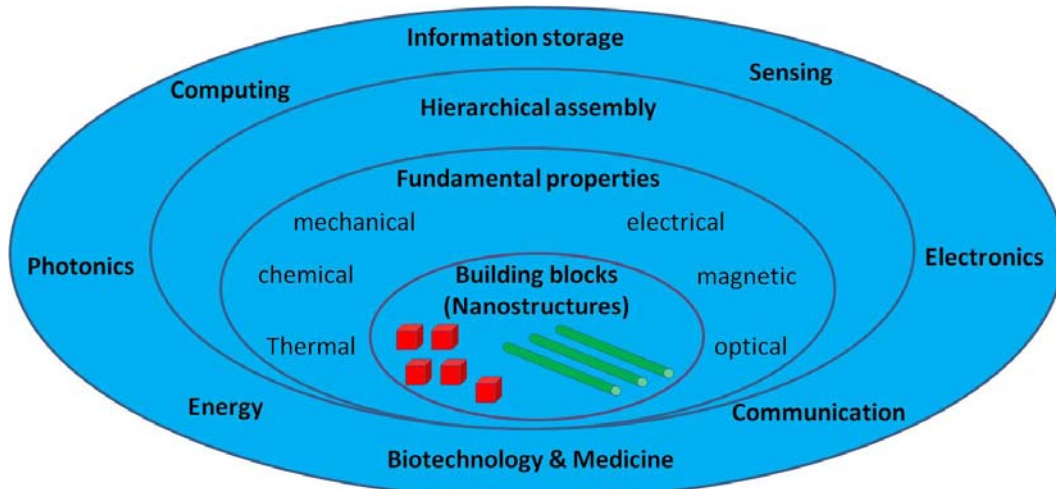


Figure 1.1: Overview of the bottom-up paradigm for nanotechnology (this intellectual path comes from Charles Lieber’s group).

## 1.2. Nanomaterials

Materials Science is an interdisciplinary field involving the synthesis, characterization and properties, and its applications to various areas of science and technologies. Traditional materials, such as metals, semiconductors, polymers, ceramics and others, were studied extensively in the recent several centuries. In the past two decades, significant attentions were attracted to novel advanced materials, especially

nanomaterials, due to its unique properties. When the size of a materials' structure is diminished to a nanometer scale, the phenomena at nanometer scale expose a completely new world of materials. The properties of matter at the nanoscale are no longer predictable by those observed at larger dimensions, and usually render novel macroscopic properties mainly due to the quantum confinement effect. Therefore, the science of nanomaterials investigates the relationship between the structure of materials at molecular or even atomic scale and their macroscopic properties. We can catalog the structures of nanomaterials into three categories: two-dimensional (2-D) nanostructures, one-dimensional (1-D) nanostructures and zero-dimensional (0-D) nanostructures. Those classifications refer to the size limitation at particular space dimensions. 2-D nanostructures, like thin film or quantum well, have one-dimensional size limitation, usually the thickness. 1-D nanostructures, like nanotubes<sup>4</sup>, nanowires<sup>5 6 7</sup><sup>8</sup>, nanorods and nanobelts (nanoribbon)<sup>9</sup>, have two-dimensional size limitation with macroscopic length at the other dimension. 0-D nanostructures, like nanoparticles and quantum dots, have three-dimensional space limitations. All of the three categories of nanostructures have been studied extensively in the recent twenty years, and significant discoveries and applications have been made, providing new routes to solve various challenges that human beings are facing such as energy, health care, environment and communications, etc.

### **1.3. One dimensional nanostructures**

Recent advances in the field of nanoscience and nanotechnology resulted from synthesis and characterization of nanostructures. Since the discovery of carbon nanotubes in 1991<sup>10</sup>, (quasi-)one-dimensional (Q1D) nanostructures, such as nanowires, nanobeltes, nanotubes and etc., have attracted tremendous attention due to their

unique and desired advantages. In addition to large surface-to-volume ratio, 1-D nanostructures have great potential as building blocks for a wide range of applications at nanometer scale, like electronics, optoelectronics, sensing, Micro-Electro-Mechanical system (MEMS) and others<sup>7-11</sup>. In the past two decades, numerous processes have been developed to fabricate many 1D nanostructures, mainly of inorganic nanomaterials, including single-element and compound semiconductors. For the single-element nanomaterials, carbon nanotubes (CNT), silicon (Si) / germanium (Ge) nanowires are most popular topics. For the compound semiconductor nanomaterials, III-V and II-VI groups have drawn much more attention. Metal oxide nanomaterials have also been extensively investigated<sup>12</sup>; typical examples include ZnO, In<sub>2</sub>O<sub>3</sub>, Ga<sub>2</sub>O<sub>3</sub>, SnO<sub>2</sub>, Fe<sub>2</sub>O<sub>3</sub>, Fe<sub>3</sub>O<sub>4</sub>, CuO, CdO, TiO<sub>2</sub>, and V<sub>2</sub>O<sub>5</sub>.

#### **1.4. One-dimensional ZnO structures**

ZnO is one of the important metal oxide semiconductors, which has a direct wide band gap of 3.37 eV and a large excitonic binding energy of 60 meV at room temperature<sup>13</sup>. In recent decade, ZnO had attracted great interests and had broad applications in optoelectronics<sup>14</sup>, logic circuits<sup>15</sup>, and piezoelectric devices<sup>16</sup>, novel field emission and others. ZnO also has unique catalytic and photocatalytic properties, which can be used to develop novel catalysis for energy production. In addition, since ZnO is biocompatible, biodegradable and non-toxic<sup>17</sup>, it has great potential in biomedical applications, such as biochemical sensing and nanomedicine.

##### **1.4.1. Synthesis of 1-D ZnO nanostructures**

ZnO nanostructures possess plentiful morphologies. 1D ZnO nanostructure have been synthesized by using various techniques. All the synthesis methods can be categorized into either chemical method or physical method. Chemical methods include

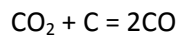
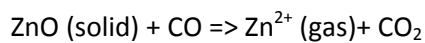
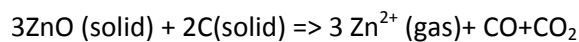
metalorganic chemical vapor deposition (CVD), aerosol processing, sol-gel synthesis, and etc. For physical methods, it includes thermal evaporation, laser ablation, electro-deposition and etc. For most chemical methods, their advantages are that chemical methods can usually produce nanomaterials with a considerable large yield. However, the surfaces of those as-grown nanostructures are always coated/contaminated by lots of polymers during the synthesis process, which affect surface properties and limit the further applications, especially for applications of surface functionalization and development of catalysts. Physical Vapor Deposition (PVD) is a thermal evaporation-deposition process belongs to the category of physical synthesis method. PVD method is popular and widely used by many research groups because of its simplicity and low economical cost. More importantly, like other physical method, PVD method can produce the nanostructures with extremely "clean" surfaces. However the amount of as-grown product is always few, which cannot satisfy the needs from the industry.

Almost all of ZnO nanostructures reported so far can be synthesized by thermal evaporation-deposition processes, which include both PVD and CVD methods. PVD and CVD are from two different categories, but they have many similarities, especially for their similar instrumental set-up. The reactions of both PVD and CVD take place in a horizontal tube furnace. CVD procedure is an oxidization process, and it uses Zn metal as source materials, and mixture of argon and oxygen as carrier gas. PVD method uses ZnO and carbon black (optional) as source materials, and pure argon as carrier gas. Pure ZnO has a high melting point (1975°C), but can be vaporized much lower than 1975°C. If only pure ZnO powders are used as source materials, the ZnO source can be evaporated if it is heated above 1300°C. ZnO will evaporate and decompose into  $\text{Zn}^{2+}$  vapor and  $\text{O}^{2-}$  vapor. Following with the carrier gas to the downstream lower temperature zone,  $\text{Zn}^{2+}$

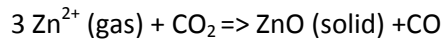
cations will nucleate with  $O^{2-}$  aions into ZnO depositing certain temperature zone with specific morphology.

If the carbon black was mixed into ZnO powders as source materials, ZnO can be vaporized lower than  $1000^{\circ}C$ . The carbon-assisted ZnO evaporation-decomposition process is complicated and its detailed reactions are still not very clear so far, but it is considered as a reduction-oxidization process following by the reactions below:

At high temperature zone (source region):



At low temperature zone (substrate region):



In regards of the reaction pressure during, CVD method usually doesn't use pumping system to pump the inner tube, comparing with common PVD system there is pumping system applied. For the most of reported nanostructures grown by PVD method, the pumping system was used for the synthesis process. However, on the basis of a lot of our pervious experiments, it shows that pumping system is not necessary and critical for the synthesis of ZnO nanostructures. Almost all the common nanostructures, including ZnO nanowires and nanobelts, can still be synthesized by the PVD method under the pumping-free system. More important, by eliminating one typical hard controlled parameter (pressure control), we found that no-pumping during the synthesis process can promote high-yield growth, which is significant for the catalysis research in our group, even through to the industry utilizations.

#### ***1.4.1.1. The system set-up of physical vapor deposition***

The horizontal tube furnace is a major part of the whole system. A Quartz or alumina tube is usually inserted into the furnace. The source material is in the combustion boat and the boat is placed in the middle of the tube where the temperature will be highest. The two sides of the tube are sealed by the stoppers. The carrier gas, usually argon or nitrogen, is provided from the upstream side. The source region (middle of the tube) is usually heated above 800°C in order to evaporate the ZnO into vapor phase. With the flowing of the carrier gas, the ZnO vapor flow downstream and deposited on the substrates at desired temperatures. Generally, for the PVD method, a pump system to pump down the vacuum inside the tube and a water cooling system to cool down the tube are also applied. A modified PVD system for nanostructure synthesis developed at UM-St. Louis was used in this thesis, as shown if figure 1-2.

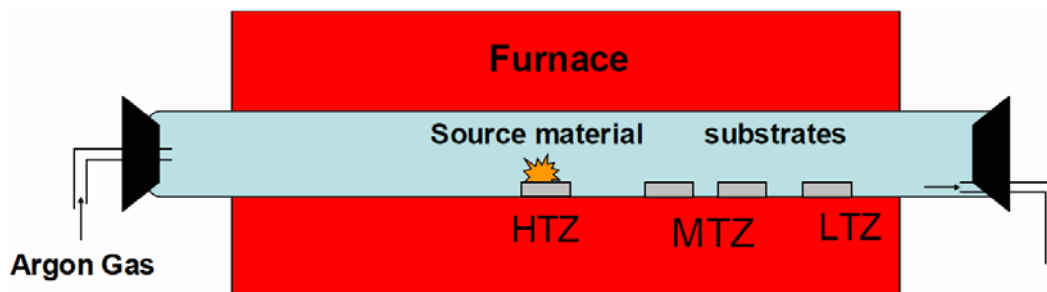


Figure 1-2: diagram of the PVD method for ZnO nanostructures synthesis in this thesis

There are two growth modes involved in the synthesis process of ZnO nanostructures. One is the well-known Vapor-Liquid-Solid (VLS) growth<sup>18 19</sup>, and the other is the Vapor-Solid (VS) growth process<sup>20</sup>. The VLS mechanism is a catalyzed growth process. A metallic or alloy catalyst, such as Au particles, had to be involved which led the growth along a specific direction to form 1D nanostructures. This process contains three steps: the dissolution of deposition materials vapor in the catalysts liquid droplets at local temperature, saturation of deposition materials in liquid droplets, then precipitation of

solid deposition materials along specific directions. The VS mechanism is a self-catalyzed process, and its details are still unclear so far. For our ZnO nanostructure growth, it is believed that Zn plays the role as a catalyst, and promotes the ZnO grown along a specific direction.

The ZnO nanostructures discussed in this thesis are believed to be grown via the VS or self-catalyzed mechanism, since no liquid or solid catalysts were present.

#### ***1.4.1.2. 1-D ZnO nanostructures' synthesis by physical vapor deposition***

The family of 1-D nanostructures has a variety of morphologies due to its unique wurtzite structures, which will be discussed in detail in Chapter 2 of this thesis. Since the first report about synthesis of ZnO nanowires by Yang et al in 2001, various morphologies of 1D ZnO nanostructures were reported such as nanowires, nanobelts<sup>9</sup>, nanorings<sup>21</sup>, nanohelices<sup>22</sup>, etc. Besides those, many Q1D complex ZnO nanostructures, such as hierarchical nanostructures, have also been synthesized and investigated<sup>23</sup>. Branched, tree-like structures or other types of complex ZnO architectures can be generated by secondary-growth on the prism surfaces<sup>24 25 26</sup>, self-assembly of nanocrystallites or defect-controlled nucleation<sup>27</sup> and growth<sup>28 29</sup>.

In the recent three years, our group (Dr. Jingyue Liu's group) concentrated on the synthesis of 1-D nanostructures. Various morphologies had been synthesized by using PVD method, preformed by several students in this group, Dr. Jinfeng Wang, Justin Paoli, Shuang Liu and Dinghao Tang.

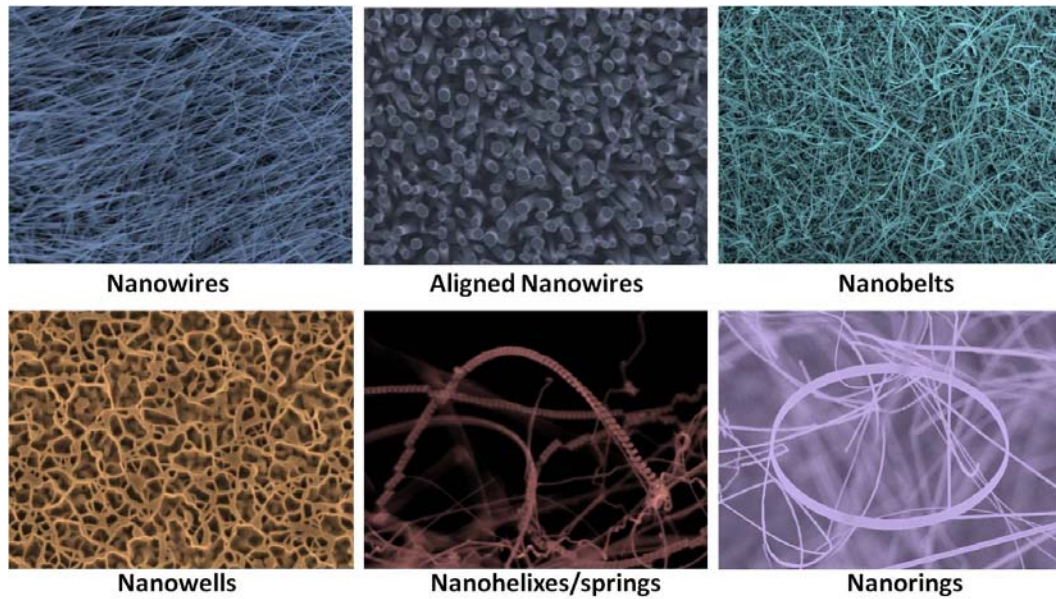


Figure 1.3: various morphologies of ZnO nanostructures grown in Dr. Jingyue Liu's group at UMSL. (images acquired and provided by Dr. Jinfeng Wang, Shuang Liu, Paoli Justin and Dinghao Tang)

#### **1.4. Goals of the thesis**

This thesis mainly focuses on the synthesis and characterization of one-dimensional Zinc Oxide nanostructures. Based on the previous experiences on the synthesis of ZnO nanostructures, the synthesis system and conditions were modified for growing complex 1-D ZnO nanostructures. The detailed understanding of the crystallography of ZnO wurtzite structure will be presented in Chapter 2. I have synthesized two types of complex 1-D ZnO nanostructures: the nanopyramid decorated ZnO nanowires and the grooved ZnO nanowires. The synthesis processes, the morphological and structural characterization of the novel nanostructures, as well as their nucleation and growth mechanisms will be presented in chapter 3 and chapter 4.

## Chapter 2. Fundamentals of Zinc Oxide

### 2.1. Introduction to crystallography

Basic knowledge of crystallography, such as, unit cell, space symmetry, crystal group, lattice constant, planes and directions, etc., is critical to understanding crystalline materials. Crystal directions and planes are important for describing the morphology of nanostructures and their growth processes. Generally, the direction of a crystal is specified by a three-number index  $[uvw]$  where  $u$ ,  $w$  and  $v$  are vector coordinates, representing a specific direction in real space, and  $\langle uvw \rangle$  indicates a family of directions. Crystal planes are described by a miller index  $(hkl)$ ; the value of the  $hkl$  is given by  $h: k: l = 1/p: 1/q: 1/r$ , where the  $p$ ,  $q$ ,  $r$  are coordinate positions that a specific plane intercepts coordinate axes at  $p$ ,  $q$ ,  $r$ .

### 2.2. Expressions of lattice directions and crystal planes for ZnO wurtzite structure

#### 2.2.1. Miller-Bravais 4-D coordinates for lattice directions and crystal planes of ZnO wurtzite structure

In the physics of crystallography, there are seven crystal systems and fourteen Bravais lattices. For most crystal systems, Miller indices are used to describe the crystal planes by the three-dimensional coordinates  $(a, b, c)$ . Yet, for the hexagonal system, such as ZnO wurtzite structure, the crystal planes are commonly referenced by a four-dimensional coordinate system  $(a_1, a_2, a_3, c)$ , where  $a_3 = -(a_1 + a_2)$ . The figure below illustrates both the 3-D coordinate system for Miller indices and the 4-D coordinate system for Miller-Bravais indices. The "c" axis in the 4-D system is the same with the "c" axis in the 3-D system. Yet the other three new axes "a<sub>1</sub>", "a<sub>2</sub>" and "a<sub>3</sub>", which are in the same plane, are different from the axes of "a" and "b" in the 3-D system. The angles between each pair of the three axes are 120°.

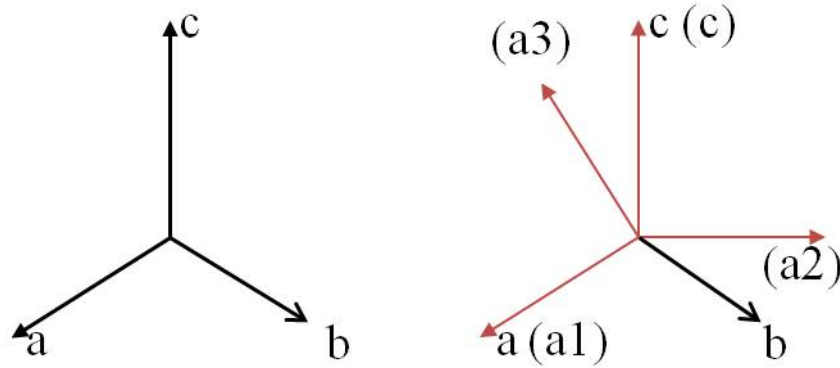


Figure 2.1: (left) a-b-c three dimensional coordinated system for Miller indices; (right) a1-a2-a3-c four dimensional coordinated system for Miller-Baravis indices.

### 2.2.1. Conversions of lattice directions and crystal planes between 3-D coordinate and 4-D coordinate

In 3-D coordinates, the direction of direct lattice or zone axis vectors is denoted by  $[u, v, w]$ , and of planar normal vectors denoted by  $(h, k, l)$ . However, for the hexagonal lattice structure, such as ZnO wurtzite, its directions and planar normal vectors are usually indexed by a set of four-index schemes designed to highlight their underlying symmetry. The conversions of lattice directions and planar normal vectors between the 3-D coordinates and the 4-D coordinates are useful for the study of materials possessing hexagonal lattice, such as ZnO, GaN and etc. It is important to note that the conversions of lattice directions and planar normal vectors between the 3-D coordinates and the 4-D coordinates are different. For converting the lattice directions between  $[u, v, w]$  in 3-D system and four index  $[h, k, -h-k, w]$  in 4-D system, the following formulae can be used:

$$h = \frac{1}{3}(2u - v); k = \frac{1}{3}(2v - u).$$

For the conversion of crystal planes in real space between  $(h, k, l)$  in 3-D coordinate and  $[a_1, a_2, a_3, c]$  in 4-D system, the formulas are:

$$a_1 = h; a_2 = k; a_3 = -(h+k); c = l.$$

The table below lists some common conversions for hexagonal lattices' directions and planar normal vectors between 3-D coordinates and 4-D coordinates<sup>30</sup>.

Lattice direction [uvw] in 3D	planar normal vector (hkl) in 3D	planar normal vectors in 4-D	Lattice direction (hybrid zone) in 4D
[uvw]	(hkl)	$[(2u-v)/3, (2v-u)/3, -(2u-v)/3-(2v-u)/3, w]$	(h, k, -h-k, l)
[00w]	(00l)	[000w]	(000l)
[21w]	(10l)	[10-1w]	(10-1l)
[12w]	(01l)	[01-1w]	(01-1l)
[1-1w]	(11l)	[1-10w]	(1-10l)
[33w]	(11l)	[11-2w]	(11-2l)
[0-3w]	(1-2l)	[1-21l]	(1-21l)
[-30w]	(-21l)	[-211l]	(-211l)

Table 2.1: Conversions of lattice direction and crystal planes between 3-D coordinates and 4-D coordinates.

There are several advantages of using the 4-D coordinate indices to describe hexagonal systems like ZnO wurtzite. In the 4-D coordinate index system, for either direction or plane, the sum of the first three indices must be zero. The plane or direction does not exist if the sum of the first three indices is not zero. More importantly, no matter how the first three indices are arranged, the specific plane or direction is always in the family of equivalent plane or direction. For instance, (10-10), (-1010), (01-10), (0-110), (1-100), (-1100), anyone of those six planes is equivalent with the rest of the five planes, and they belong to the same family of {10-10}. Therefore, for a hexagonal system, directions and planes represented by the 4-D coordinate indices describe the three-fold symmetry of the hexagonal system.

## 2.2. Basic crystallography of Zinc Oxide

Zinc Oxide is one of the most important semiconductor materials in the metal oxide family. The most common crystal structure of ZnO is the non-centrosymmetric wurtzite structure. It is categorized as a hexagonal Bravais lattice with the lattice constants of  $a=0.3296$  nm, and  $c=0.52065$  nm, belonging to the space group of  $P6_3mc$ . ZnO wurtzite structure has  $6mm$  point group symmetry, where "6mm" is the Herman-Mauguin crystallographic nomenclature used to describe the 6 mirror planes within the basal plane of the crystal.

ZnO wurtzite structure is composed of a number of alternating planes with tetrahedrally-coordinated  $O^{2-}$  and  $Zn^{2+}$  ions, stacked along the  $c$ -axis. Although the entire unit cell of ZnO wurtzite is neutral, the arrangement of the Zn cations and O anions can result in charged surfaces. Some surfaces can be terminated entirely by Zn cations or O anions, which resulting in positively or negatively charged surfaces. Here, we call those types of surfaces "polar surfaces". The positively charged  $Zn^{2+}$  (Zn-(0001)) surface and the negatively charged  $O^{2-}$  (O-(000-1)) surfaces are polar surfaces. Additionally, there are several (semi-) polarized surfaces in the ZnO wurtzite structure, such as  $\{10-11\}$ ,  $\{11-21\}$ , etc. Parallel with the  $c$ -axis, ZnO- $\{10-10\}$  and ZnO- $\{11-20\}$  are the two most stable neutral surfaces in the ZnO wurtzite structure.

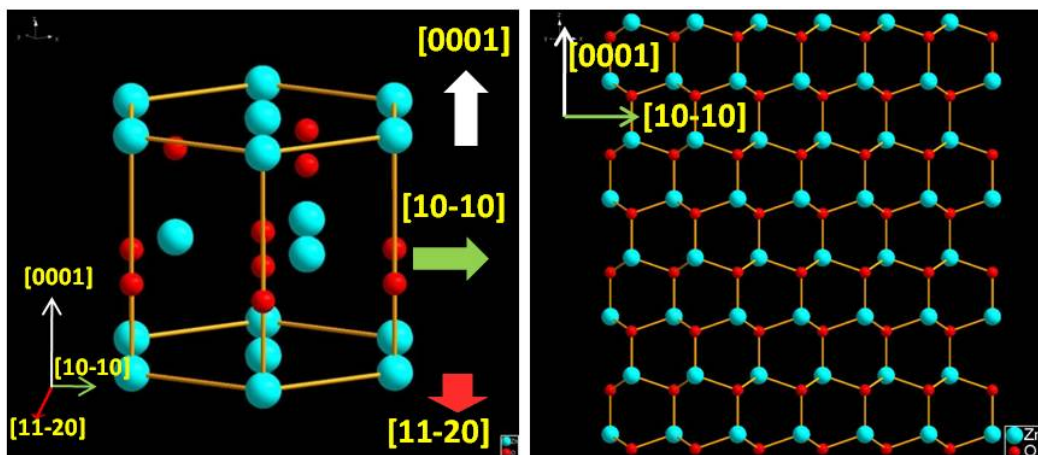


Figure 2.2: ZnO wurtzite structure. (left) crystal structure model of wurzite ZnO; (right) atomic profile images of wurzite ZnO along  $\langle 11-20 \rangle$ .

Based on the surface charge distribution, the ZnO crystal surfaces can be classified into non-polar surfaces or (semi-) polar surfaces. In the family of ZnO nanostructures, the ZnO crystal surfaces of (0001), {10-11} and {11-22} are typical polar surfaces, and ZnO {10-10}, {11-20}, {10-12} are typical non-polar surfaces, as shown in the figure below and indicated in the ZnO hexagonal wurtzite model.

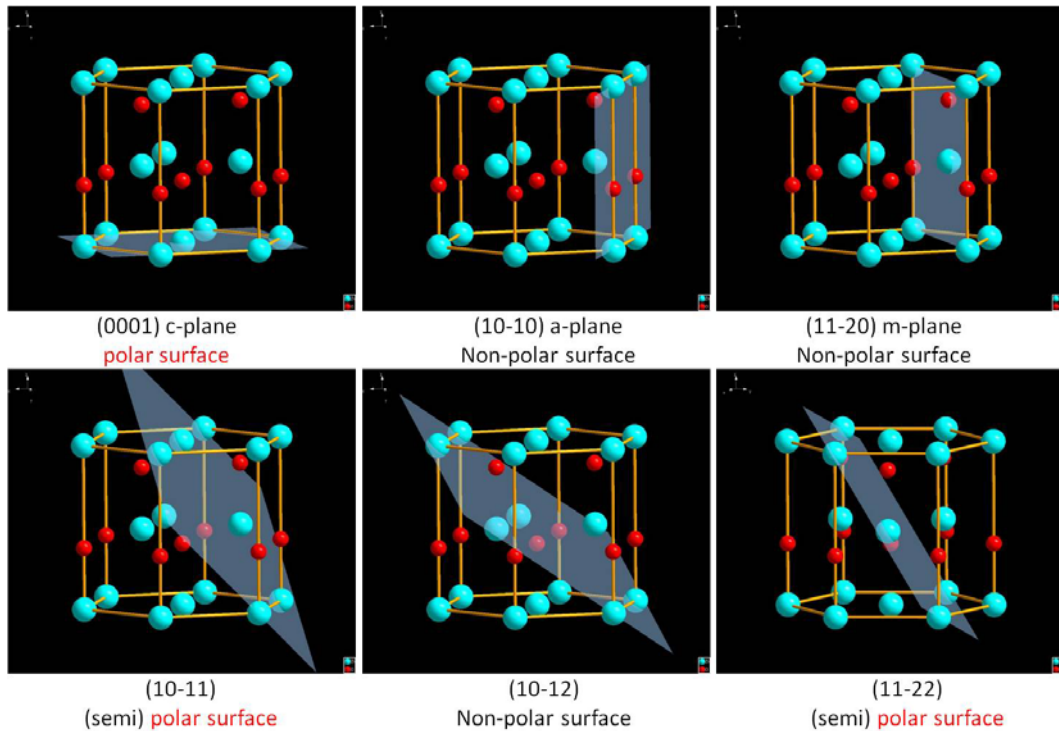


Figure 2.3: Some important crystal planes in ZnO wurtzite structure

The atomic arrangement of the ZnO wurtzite structure projected along the [11-20] direction is shown in the figure below. Besides the most typical (0001) and (000-1) polar surfaces, ZnO-{10-11} are also terminated by Zn cations or O anions, which are another typical polar surfaces in the ZnO wurtzite structure. For the ZnO-{10-10} and {10-12}

crystal surfaces, each  $\text{Zn}^{2+}$  is neutralized by a  $\text{O}^{2-}$  so the ZnO {10-10} and {10-12} are typical non-polar surface. All those surfaces are depicted in the ZnO hexagonal wurtzite model as shown in the right figure below.

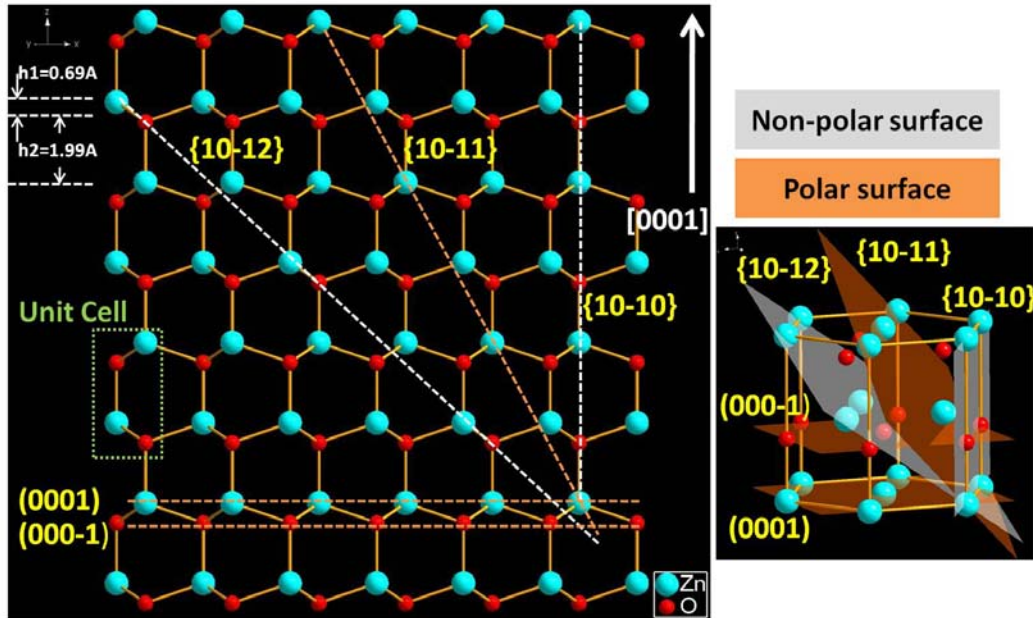


Figure 2.4: (left): ZnO wurtzite structure projected along  $\langle 11-20 \rangle$ ; (right): the (semi-)polar and non-polar surfaces along  $\langle 11-20 \rangle$  zone axis.

By projecting ZnO wurtzite structure along  $\langle 10-10 \rangle$ , the typical  $(000\pm 1)$  surfaces can be clearly observed. In addition, ZnO-{11-20} surfaces are another non-polar surfaces having similar electron distribution with those of the {10-10} surfaces. ZnO {11-21} are another typical (semi-)polar surfaces which are similar to the {10-11} surfaces. All the surfaces mentioned in this paragraph are depicted in the ZnO hexagonal model in the figure right below.

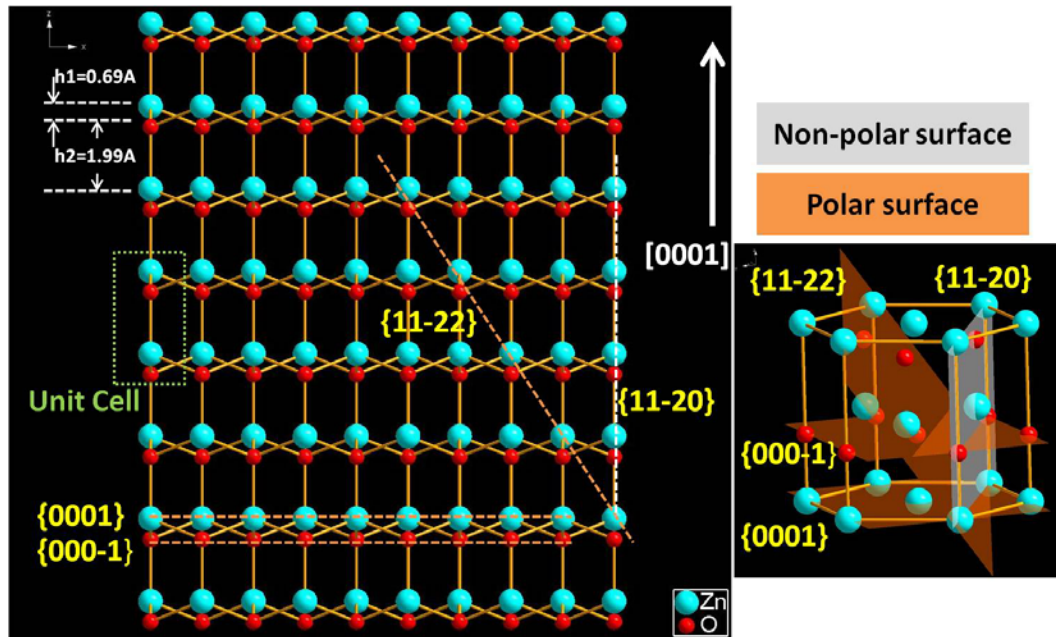


Figure 2.5: (left): ZnO wurtzite structure along the zone axis of  $\langle 10\bar{1}0 \rangle$ ; (right): the (semi-)polar and non-polar surfaces along  $\langle 10\bar{1}0 \rangle$  zone axis.

### 2.3. Characterization techniques

The sizes of the synthesized nanostructures are so small that Electron Microscopy (EM) techniques have to be used to visualize them. The X-ray diffraction (XRD) technique is also used to characterize the phases and the sizes of the synthesized ZnO nanostructures. Field-emission scanning electron microscope (FE-SEM), scanning transmission electron microscope (STEM), energy-dispersive X-ray spectroscopy (EDS) attached to the SEM and X-ray diffraction (XRD) are used to characterize the synthesized nanostructures.

FEG-SEM and STEM are two of the most powerful tools for characterizing nanostructures. In the following paragraphs, a brief introduction to these unique instruments is described.

### **2.3.1. Electron Microscopy**

“Seeing is believing”. So far, electron microscopy is the only method to provide a way for us to see the structures of nanomaterials (particles, wires, belts, etc.) directly at a nanometer or even sub-angstrom scale.

Electron microscopy was developed in the early 20th century. In the recent thirty years, various advances in electron microscopy techniques were achieved, especially for High Resolution Electron Microscopy (HRTEM), which provides a powerful tool to observe phenomena at nanometer scale or even at the sub-angstrom scale in some cases.

The principles and the operating procedures of SEM and STEM have similarities. The figure below shows the main components of a typical modern SEM or STEM.

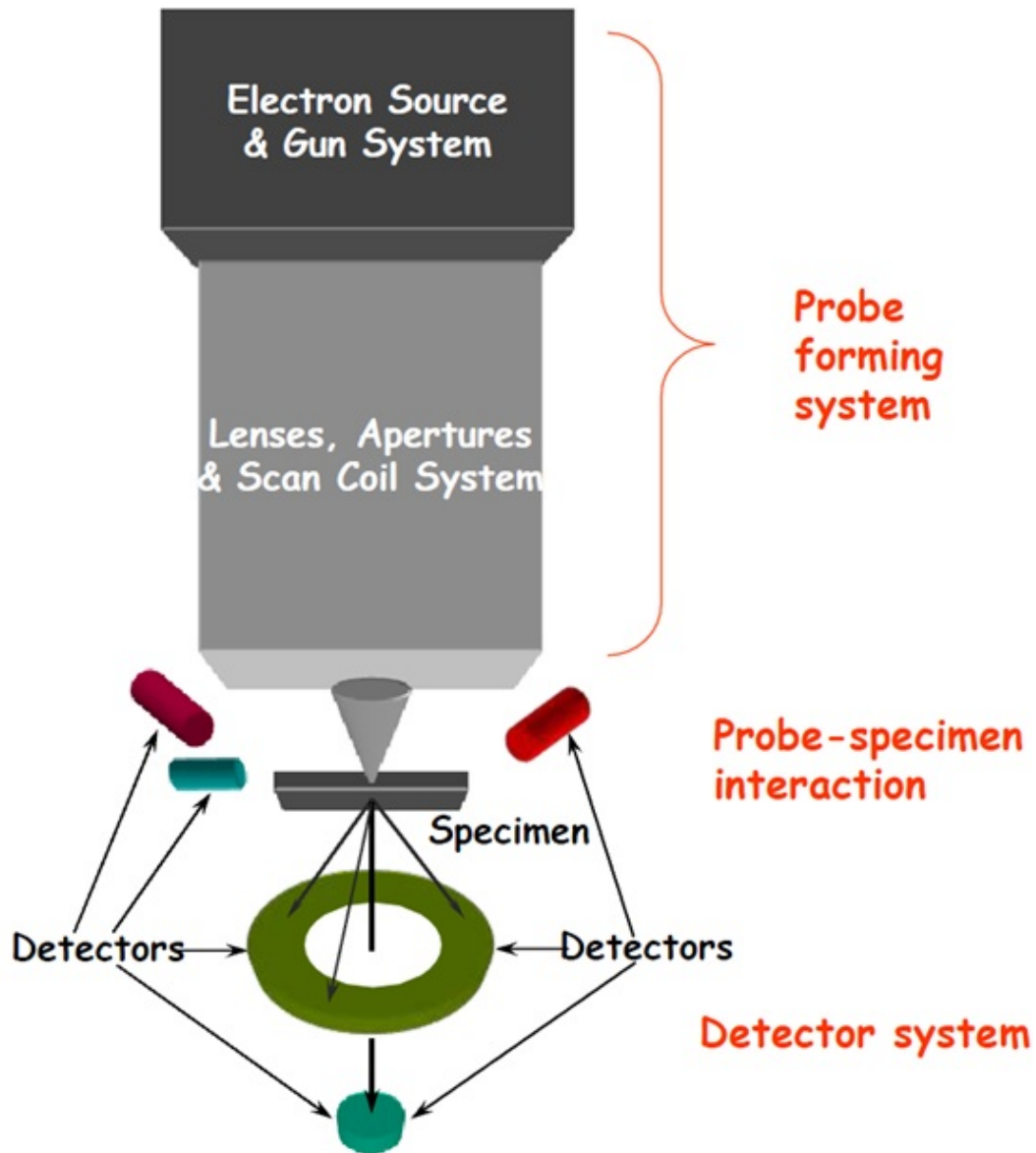


Figure 2.6: schematic diagram illustrates the main components of modern SEM/STEM (from Professor Jimmy Liu's lecture notes)

Generally, a typical scanning (transmission) electron microscope contains an electron source, a probe forming system, a sample holder system and detector systems. The function of the electron source---the electron gun---is to provide an intense beam of electrons with a small probe size. There are two major types of electron guns: thermionic electron gun and field emission electron gun. The field emission gun has

many advantages, like high electron emission current and beam brightness, smaller source size, lower energy spread, great stability and long life time.. Therefore, electron microscopes equipped with a field emission filament is ideal for high coherence lattice imaging and high spatial resolution microanalysis. The probe forming system consists of a series of electromagnetic lens and coils, generating a tinny probe size. The probe size in SEM/STEM determines the limit of image resolution.

The process of electron beam interacts with sample is quite complicated. Usually, the interaction between electron beam and a bulk sample will generate various signals, such as secondary electrons, backscattered electrons, X-rays, auger electrons, light, transmit electrons and etc. The various signals provide useful information of the sample, which can be acquired by various sample detectors in the detectors system. For SEM, the major detectors are secondary electron detectors, backscattered electron detectors. Secondary electron images provide excellent resolution and high surface sensitivity, which is the best to characterize nanostructures' morphology and their fine structures. Backscattered electron is sensitive to atomic number, which is excellent to characterize the atomic difference in the specimen. For the modern STEM, high-angle annular detector is the most powerful detector for atomic resolution images. In addition to these imaging techniques, X-ray energy dispersive spectroscopy (EDS) and electron energy loss spectroscopy (EELS) are also useful techniques for extracting chemical information of the specimen.

#### **2.4. General understanding of ZnO 1-D nanostructures**

ZnO nanocrystals have three fastest growth directions,  $(000\pm 1)$ ,  $\langle 11-20 \rangle$  and  $\langle 10-10 \rangle$ . Due to those three fastest growth directions and kinetic growth conditions, ZnO wurtzite crystallites are three dimensional objects with well-defined, low-index

crystallographic faces. The figure below shows a few typical morphologies of 1-D ZnO wurtzite structure. Those 1-D ZnO nanostructures usually have two major categories of morphologies: wire-like and belt-like. ZnO  $\{10\bar{1}0\}$  and  $\{11\bar{2}0\}$  planes tend to dominate the surfaces of the nanostructures due to their lower surface energy. ZnO nanowires usually were enclosed by six side surfaces, ZnO  $\{10\bar{1}0\}$  or  $\{11\bar{2}0\}$ , reflecting the hexagonal symmetry of ZnO wurtzite structure (figure (a)). ZnO nanobelts have three surface configurations, as shown in figure (b-c). (b) and (c) configurations are mainly dominated by non-polar surfaces of  $\{10\bar{1}0\}$  and  $\{11\bar{2}0\}$ . (d) is dominated by the polar surfaces, which can be grown by introducing planar defects parallel to the polar surfaces, and which are rare among all the configurations. Yet, this configuration is critical for the formation of nanoring and nanospring's morphologies.

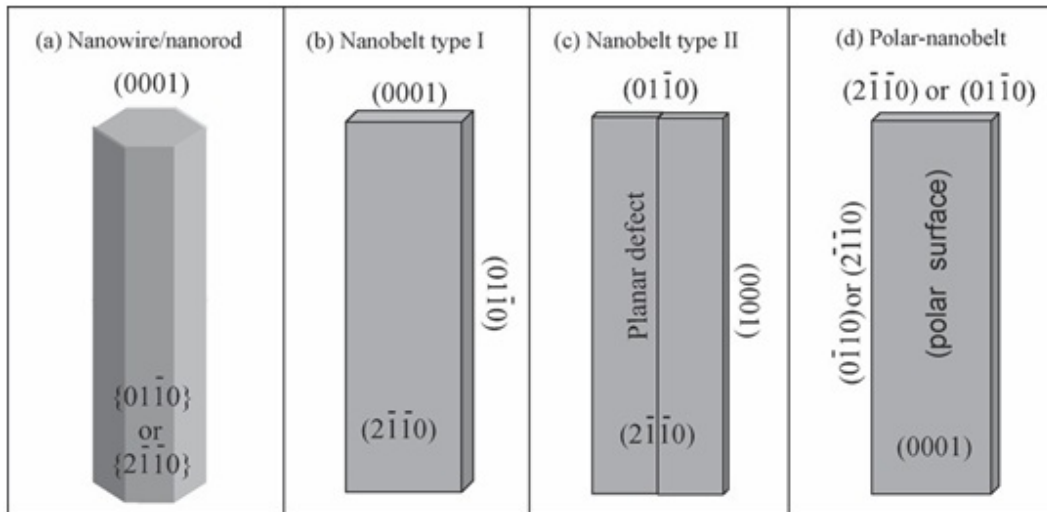


Figure 2.7: Typical growth morphologies of 1-D ZnO nanostructures and the corresponding facets.

## 2.5. Ideal candidate of 1D nanostructure for surface functionalization

1D nanostructures have been considered as ideal materials for detecting ultra-low biochemical reactions because of the high surface-volume ratio and tunable electron

transport due to quantum confinement effect<sup>11</sup>. Controlled modifications of the surface morphology and structure of 1D nanostructures are interesting since they may facilitate anchoring, functionalization or chemical reactions. So far, the most recognizable contribution to the field of biochemical detection by using 1-D nanostructures, such as single wall carbon nanotubes (SWNTs), silicon nanowires (Si NWs), conducting polymer nanowires (CP NWS) and others, has been made mainly in the field of surface functionalization including both of covalent and non-covalent methods<sup>31</sup>. Because of the neutral charged surface due to the surface energy minimization, most nanostructures possess non-polar surfaces. In order to modify chemical molecules on their non-polar surfaces, the harsh chemical surface treatment needs to be achieved<sup>32</sup>, which produces a covalent functional charged group as a molecular linker. Therefore, polar charged surface dominated nanostructures are expected to have promoting properties for surface functionalization<sup>21 33</sup>. Hereby, three key characteristics of the candidate nanoscale materials for surface functionalization should be carefully considered: (1) abundant nonbonding atoms on the surfaces; (2) surface stability, and (3) non surface contamination. Candidate nanostructures should also exhibit appropriate optical and semiconductive properties to foster the biochemical signal from surface linked probe molecules in order to promote detection at low concentrations, even at an ultratrace level. In addition, simple and straightforward synthesis should yield the successful growth. More important, these nanomaterials should be biocompatible and environmentally friendly for detection in environments that involve most biochemical interactions. Lastly, chemical reactions applicable to derivatize the surfaces of nanomaterials covalently should be widely available in order to link specific biomolecules on nanomaterials and maximize specificity of biochemical detection.

## 2.6. Kinematical SADP electron diffraction simulation

STEM characterization gives atomic scale crystalline information of the specimen. Due to its atomic resolution, selected area diffraction pattern (SADP) can be obtained by Fast Fourier Transform of the digital STEM images directly. SADP electron diffraction simulation provides a convenient way to quickly identify the zone axes of STEM images, and further to identify the crystal directions and planes of the characterized nanostructures. Three typical SADP electron diffraction simulation patterns are listed as below, along  $[0001]$ ,  $[10\bar{1}0]$ , and  $[2\bar{1}\bar{1}0]$ , respectively.

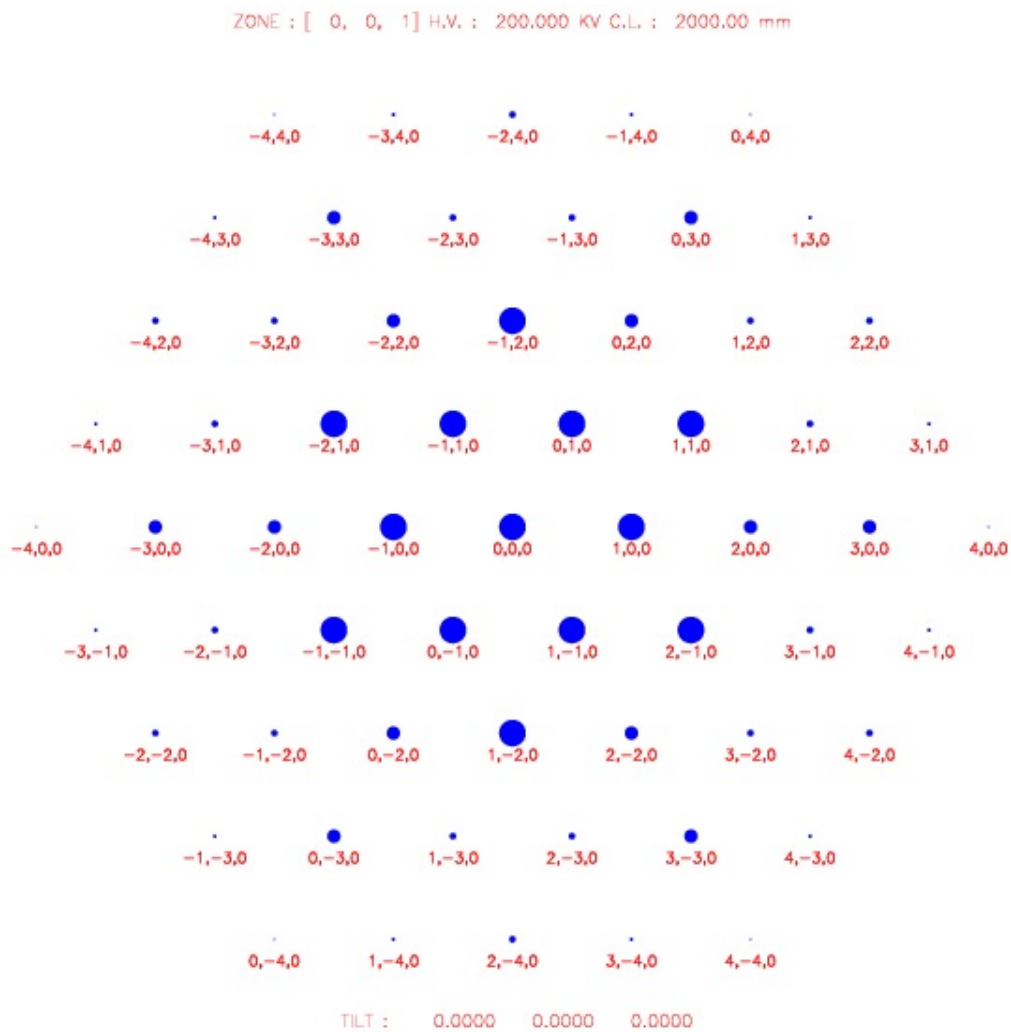


Figure 2.8: Kinematical SADP simulation pattern along  $[001]$  or  $[0001]$ .

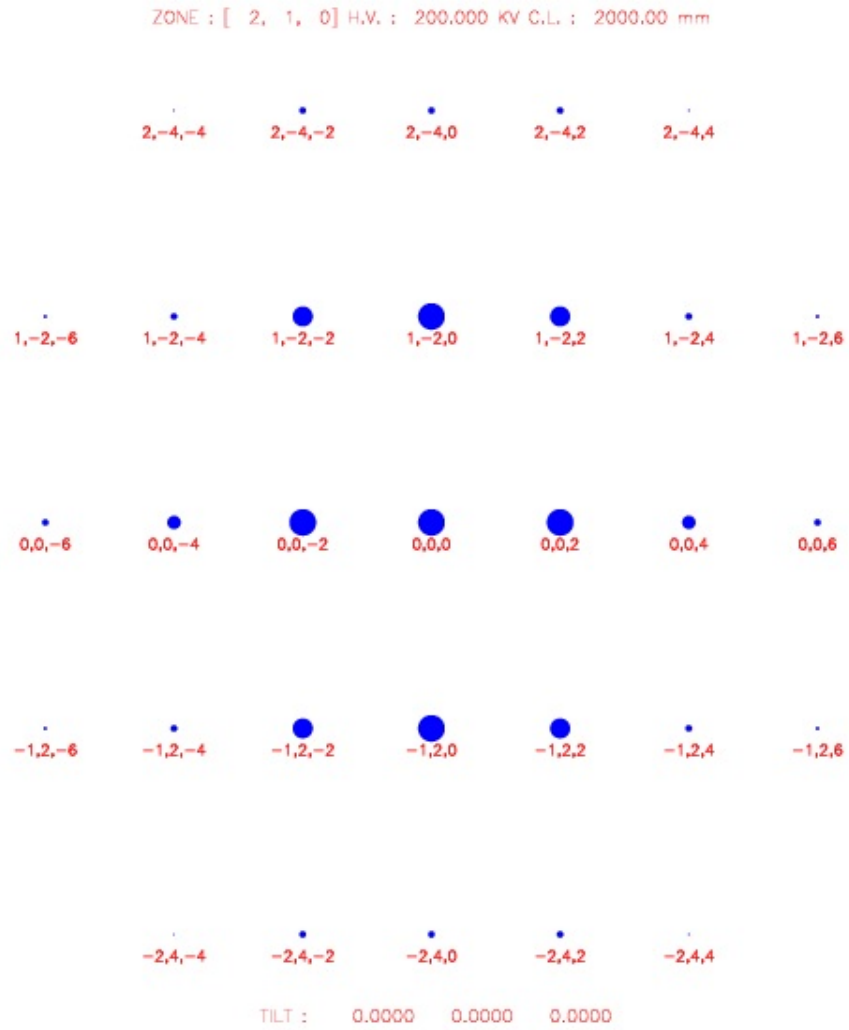


Figure 2.9: Kinematical SADP simulation pattern along [210] or [10-10].

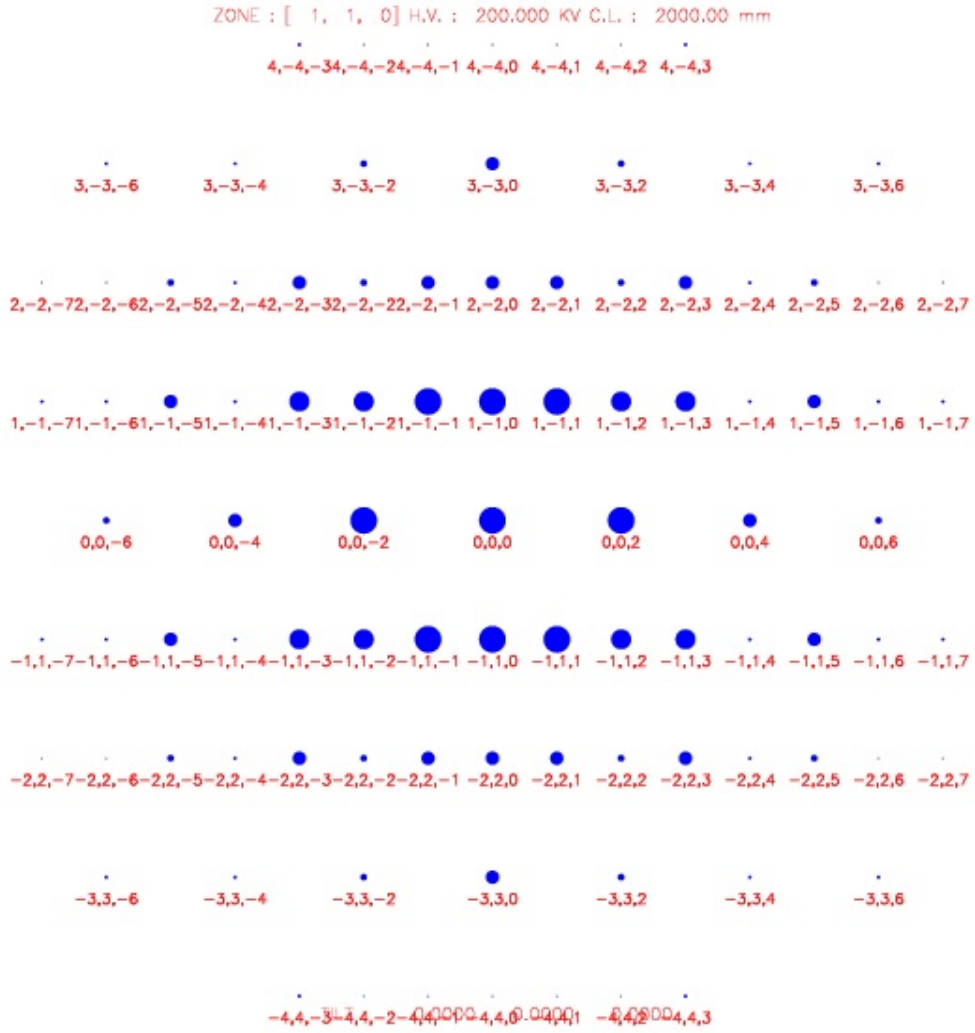


Figure 2.10: Kinematical SADP simulation pattern along [110] or [11-20].

## **Chapter 3: Synthesis and Characterization of 1D Complex ZnO Nanostructures**

ZnO nanostructures, being biocompatible, biodegradable, and less toxic, have attracted significant interests because of its potential applications in diagnostics, treatment and prevention of diseases<sup>34</sup>. One dimensional ZnO nanostructures can be functionalized by chemical or biological molecules. To make it easier to functionalize nanowires (e.g., attachment of biomolecular recognition or other types of molecules or nanoparticles onto the surfaces of nanowires), it is desirable to fabricate nanowires with rough or corrugated surfaces. Additionally, periodically faceted surfaces of nanostructures may provide novel surface properties, for example, as supporting materials for developing novel catalysts.

In this chapter, several novel morphologies of ZnO 1D complex nanostructures are introduced. All of them may have great potential for surface functionalization for applications in biosensing.

### **3.1. Synthesis and Characterization of Nano-pyramid Decorated ZnO Microwires**

In this section, we report the synthesis and characterization of nano-pyramid decorated ZnO microwires.

#### **3.1.1. Synthesis of nano-pyramid decorated ZnO microwires**

The as-grown nanostructures were synthesized in a high temperature horizontal tube furnace by a standard evaporation-condensation process (physical vapor deposition). Three grams of source material (carbon black mixed with zinc oxide powders at weight ratio of 1:2) was put in an alumina combustion boat placed in the center of a horizontal

tube furnace. Ceramic substrates were placed downstream for collecting the growth product. The inner tube was filled with oxygen/argon as carrier gas at the volume ratio of 1:19 at a flow rate of 15 sccm. The source materials were heated to 1000°C for two hours.

### **3.1.2. Characterization of nano-pyramid decorated ZnO microwires**

Both axial and radial epitaxial growths are achieved by using a standard evaporation-condensation process<sup>8</sup>. A mixture of argon and oxygen as carrier gas at proper ratio and no pumping during the crystal growth are the keys to promote both axial and radial epitaxial growths of 1D ZnO nanostructures to form complex morphology. Detailed synthesis procedure and conditions can be found at the methods part in this chapter.

The as-grown nanostructures are characterized by Field-emission Scanning Electron Microscope (FE-SEM). Low magnification SEM image shows the as-grown products are at a significant percentage, all the thick and long wires are decorated with nano-pyramids as shown in the figure 3-1(a). X-ray energy dispersive spectroscopy (EDS) indicated that the as-grown material is Zinc Oxide, as shown in figure 3-1(b).

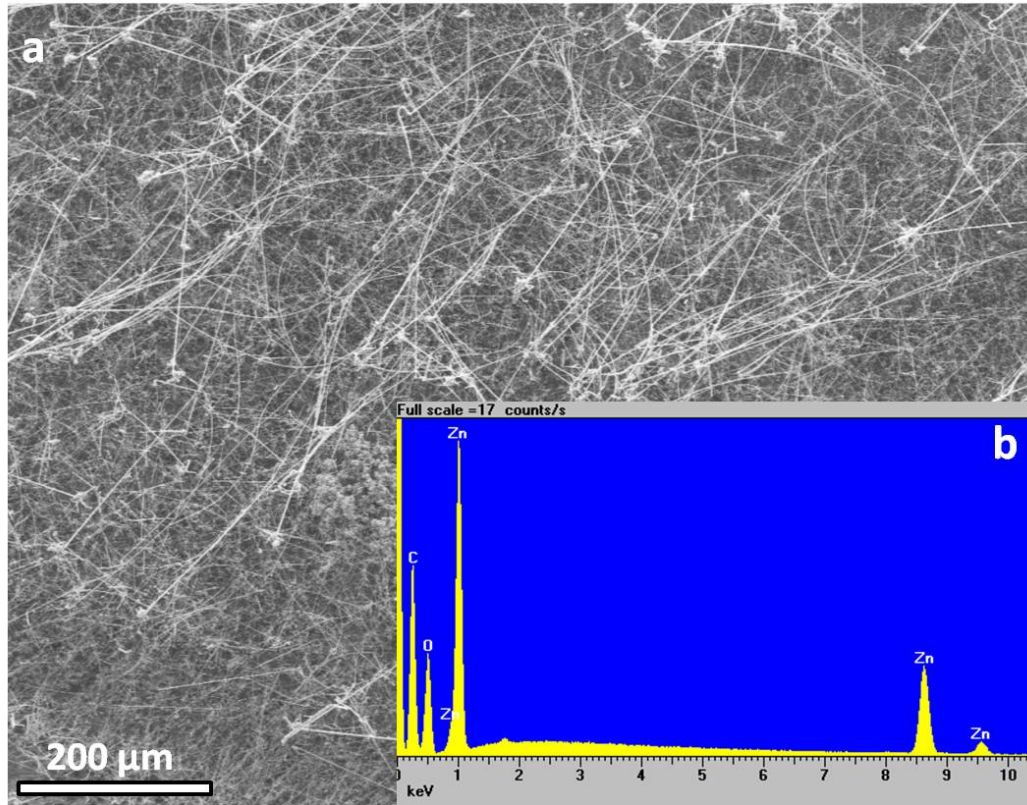


Figure 3-1: (a) low magnification SEM image shows a significant present of as-grown nanostructures. All the big wires in the image are as-grown nano-pyramid decorated microwires. (b) X-ray dispersive spectroscopy indicates the component of as-grown materials is Zinc Oxide.

Those microwires are decorated uniformly by nano-scale pyramids, as shown by the high resolution SEM image (Figure 3-2). Detailed analysis on the basis of SEM images reveals that the diameters of the nano-pyramid decorated microwires range from 0.6  $\mu\text{m}$  to 2  $\mu\text{m}$ , and their lengths range from 40  $\mu\text{m}$  up to around 1 mm. SEM images (Figure 3-2a, b and c) indicate the growth middle region, end region and the region which the nucleation was just starting, clearly revealing the hexagonal cross-section of the microwire prism.

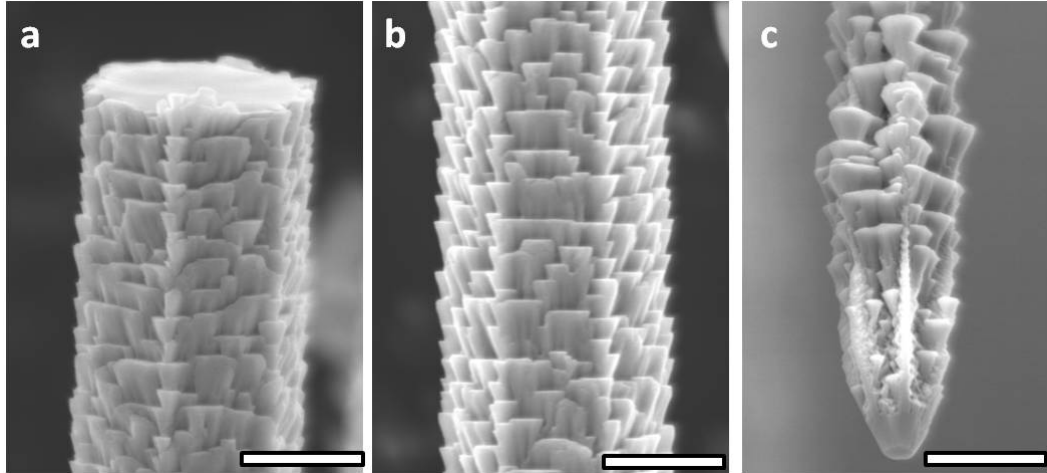
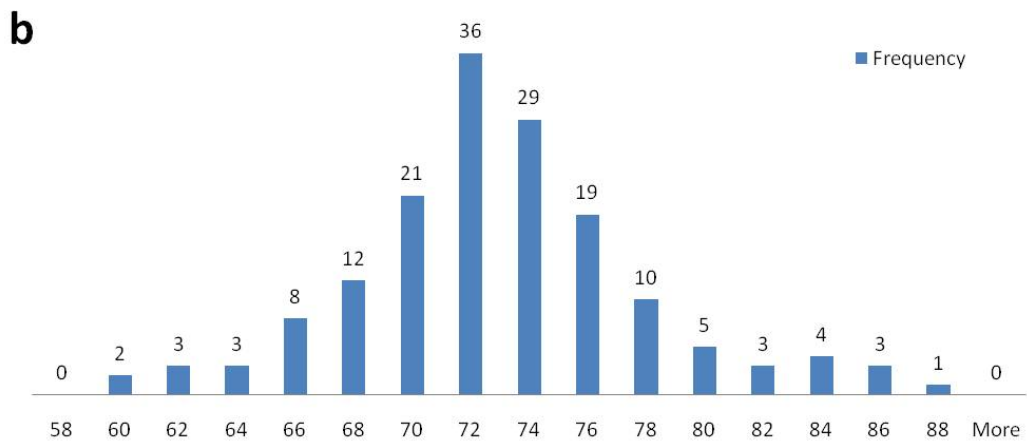
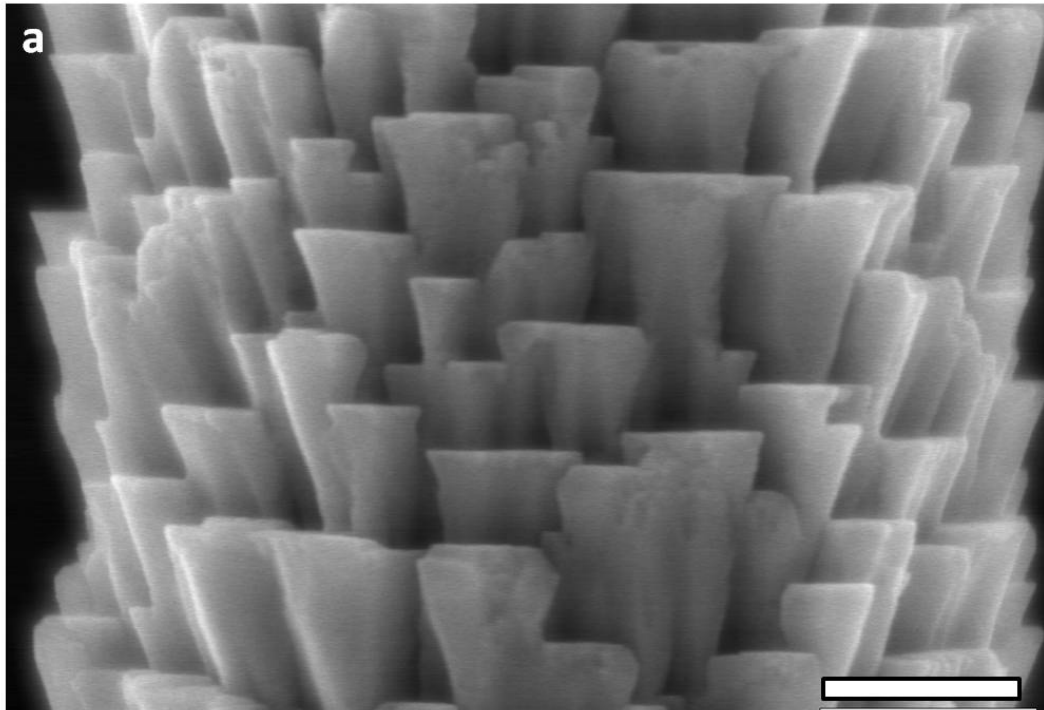


Figure 3-2: SEM images of as-grown nanostructures. (a) Medium magnification SEM image of the middle region of as-grown nanostructures showing the extremely uniform decoration of nano-pyramids standing on the nanowires prism surfaces. (b) Medium magnification SEM images of the end of as-grown nanostructure showing the flat end with the hexagonal cross-section. (c) Medium magnification of SEM image of tip region of as-grown nanostructures showing the arrow-like sharp tip. The scale bars in the figures are 500 nm. (thank Dr. J. Liu for taking the HR-SEM images)

For the decorated ZnO nano-pyramids on the prism surface of microwires, all the nano-pyramids' basal planes are perpendicular to the microwires' prism surfaces. That suggests that all the decorated nano-pyramids have ZnO (0001) or (000-1) crystal facets as basal plane, and grow along the ZnO [0001] direction, which is the same as the microwire growth direction. By analysis of the morphology of plan-view SEM images, the nano-pyramids have a width ranging from 66nm to 231nm with the mean value of 127nm. The basal angles of nano-pyramids between pyramid plane and basal plane were measured on SEM images. 169 basal angles were measured, which gave a mean value of 72°, as shown on the histogram of basal angle statistics (figure 3-3b). The mode value of 72° as the basal angle between the pyramid planes and basal plane, which suggests that the pyramid planes of the nano-pyramids are ZnO {20-21} crystal facets. The density of nano-pyramids was estimated around  $9.7 \times 10^9 / \text{cm}^2$ . The densities in axial

and azimuthal directions were also calculated, which gave  $3.5 \times 10^5/\text{cm}$  and  $3.25 \times 10^5/\text{cm}$ , respectively. In addition, the same region of as-grown nanostructures was examined by X-ray diffraction (XRD) (figure 3-4), which shows that the as-grown microwires have ZnO wurtzite structure.



**Histogram of nano-pyramid's basal angles**

Figure 3-3: (a) high resolution SEM images of as-grown nanostructures. The scale bar in the figure is 200 nm. (thank Dr. J. Liu for taking the HR-SEM images) (b) Histogram of basal angle of nano-pyramid measured by SEM images.

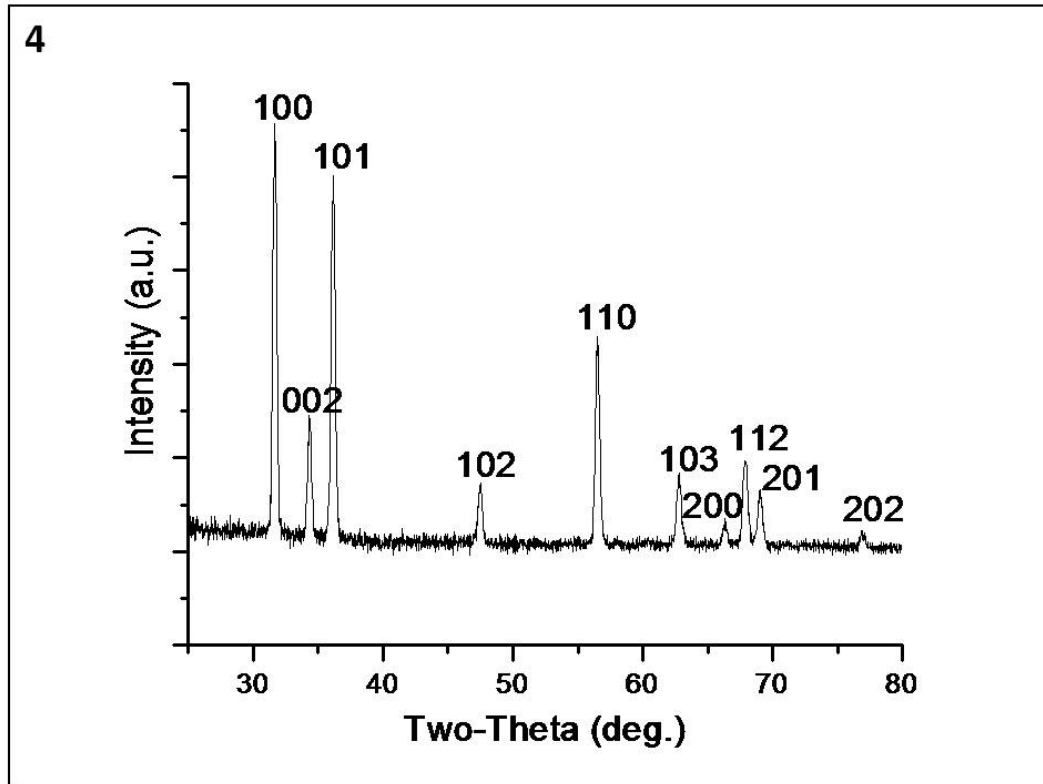


Figure 3-4: XRD spectrum of as-grown nanostructures reveals that nano-pyramid decorated nanowires have ZnO wurtzite structure.

The as-grown sample and their atomic structure were further characterized by High Angle Annular Dark Field (HAADF) imaging in Aberration-corrected Scanning Transmission Electron Microscope (Cs-corrected STEM). Because the thickness of as-grown microwires (around 1  $\mu\text{m}$ ) was too large for STEM's incident beam to penetrate, only those nano-pyramids on the left and right edge sides in plan-view STEM images could be characterized. To directly see the pyramids' surfaces the wires were projected along ZnO  $\langle 11\bar{2}0 \rangle$  directions since the directions are parallel to the both pyramid surfaces and basal surfaces of the nano-pyramids on edge sides of the wire's prism. Figure 3-5a is a low magnification high-angle annular dark-field (HAADF) image, showing a typical individual microwire modified with nano-pyramids. Figure 3-5b is a medium

magnification HAADF-STEM image shows basal angle region of a typical nano-pyramid. The inset shows the digital diffractogram by Fourier transform. All the pyramids consist of  $\{10-11\}$  and  $\{10-10\}$  facets as the transition region between basal planes and pyramid planes of the nano-pyramids. This atomic arrangement suggests that such a surface construction is stable to connect basal plane and pyramid planes. Figures 3-5c and 3-5d are the sub-angstrom resolution HAADF-STEM images showing the nano-pyramid's basal and pyramidal plane, respectively. They clearly reveal that each individual nano-pyramid has a flat (0001) basal plane. It is interesting to note that in the sub-angstrom resolution HAADF-STEM image (fig. 3-5C), there is at least one layer, sometimes two layers, of the (0001) plane that has lower intensity. The ZnO (0001) surface is atomically flat with incomplete growth of the outermost surface layer. For the pyramidal surface, with the surface steps shown clearly (fig. 3-5d) decomposes into ZnO  $\{10-11\}$  and  $\{10-10\}$  facets. The pyramidal planes are composed of polar  $\{10-11\}$  facets and non-polar  $\{10-10\}$  facets at 1:1 segments along (0001) axial axis. This combination of facets provides the  $\{20-21\}$  directions of pyramidal planes.

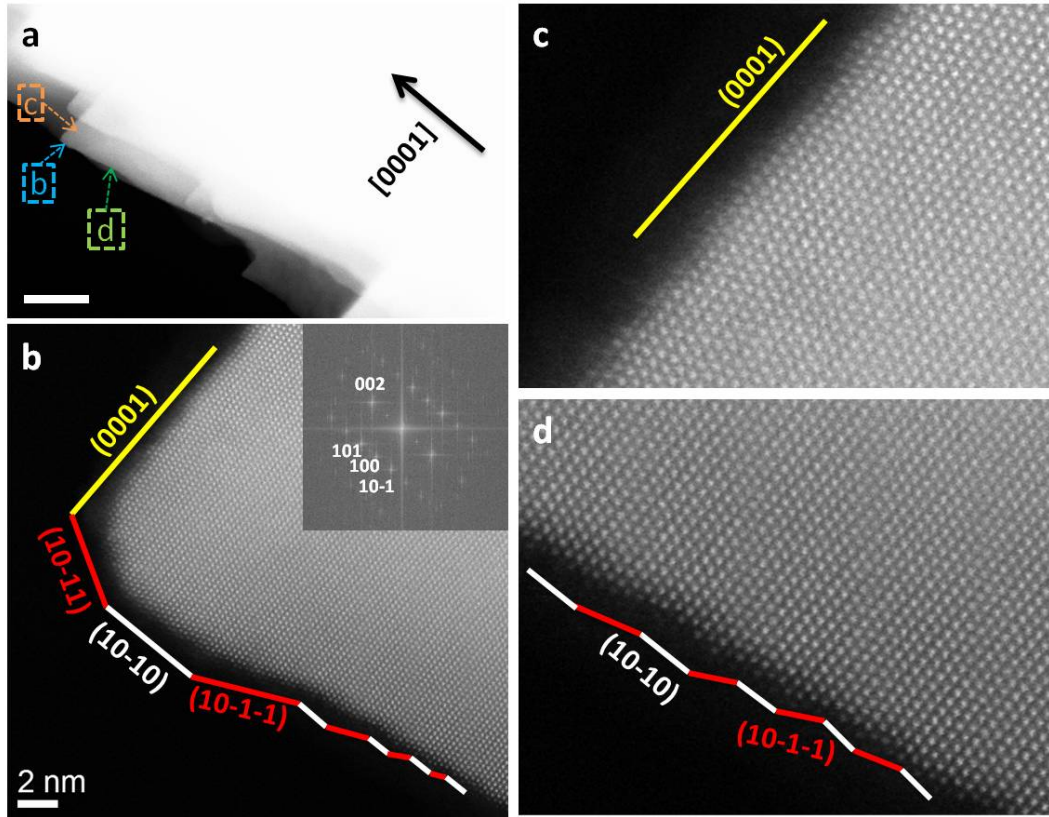


Figure 3-5: HAADF-STEM images of as-grown nanostructures with the zone axis of  $\langle 11-20 \rangle$ : (a) Medium magnification HAADF-STEM image of as-grown nanostructure; The scalar bar in the image is 50 nm. (b) sub-angstrom resolution HAADF-STEM image showing basal angle region of a typical individual nano-pyramid, revealing the (0001) crystal facet as nano-pyramid basal plane, and {10-11} and (10-10) crystal planes as translated facet between basal plane and pyramid plane, and the {20-21} as pyramids plane composed by polar {10-11} facet and non-polar {10-10} facet; (c) sub-angstrom resolution HAADF-STEM image showing the pyramid plane of a typical individual nano-pyramid; (d) sub-angstrom resolution HAADF-STEM image showing the pyramid plane of an individual nano-pyramid which has a bigger basal angle. (thank Dr. J. Liu for taking the STEM images)

Sub-angstrom resolution HAADF-STEM image (fig 3-6a) reflects another pyramidal plane with different combination of facets, revealing that the combination segments' ratio of polar {10-11} and non-polar {10-10} facets is 1:3. This combination yields the {40-41} pyramidal planes.

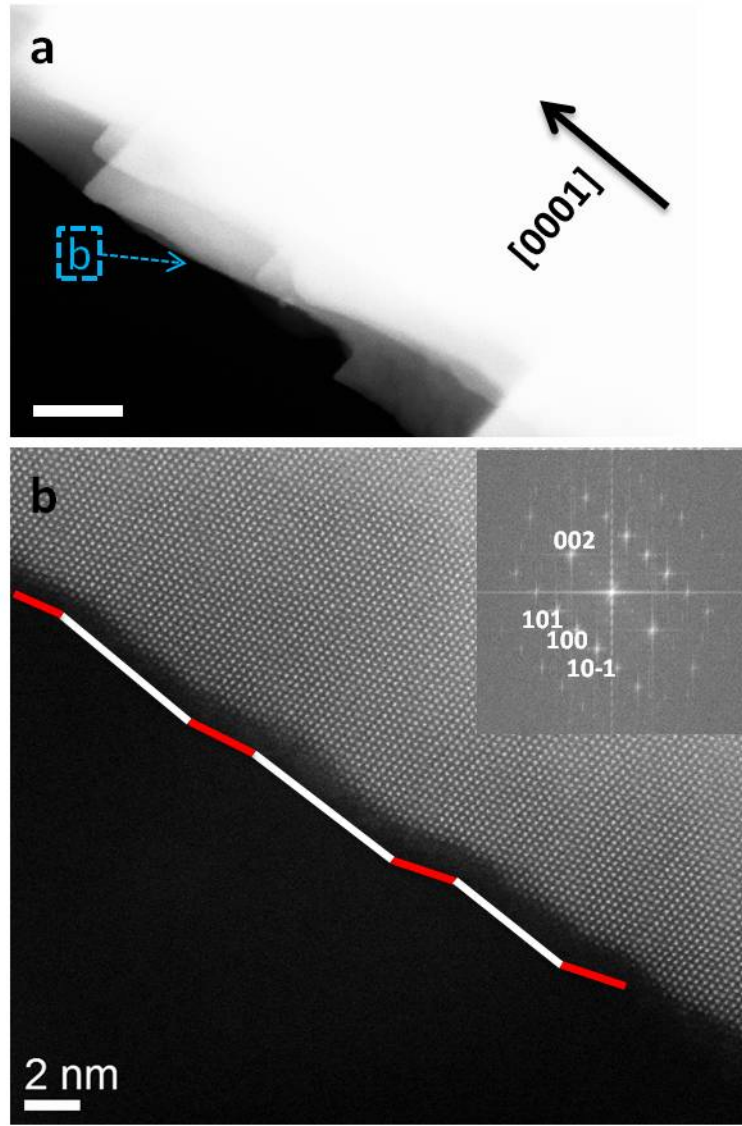


Figure 3-6: HAADF-STEM images of as-grown nanostructures with the zone axis of  $\langle 11-20 \rangle$ . (a) Medium magnification HAADF-STEM image of as-grown nanostructure; (b) sub-angstrom resolution HAADF-STEM image showing  $\{40-41\}$  planes as pyramid planes, which can be further decomposed into  $\{10-10\}$  and  $\{10-11\}$  with the ratio of 3:1. (thank Dr. J. Liu for taking the STEM images)

On the basis of STEM characterization, 25 basal angles were also measured on STEM images, as shown in the histogram (figure 3-7a). The mean value of STEM-measured basal angle was  $74.16^\circ$  and the mode value was  $75^\circ$ , which confirm the theoretical value of  $74.88^\circ$  given by the angle between ZnO crystal  $(000+1)$  or  $(000-1)$  facet and the  $\{20-21\}$

facets. The mean value of STEM-measured basal angle ( $74.16^\circ$ ) has a difference of  $2^\circ$  with the mean value of SEM-measured basal angle ( $71.99^\circ$ ). This  $2^\circ$  difference is due to a projection issue about two different zone axes. Considered by the geometry of nano-pyramid, the approximate 2 degree difference was due to the projection issue of nano-pyramid. In fact, the angles measured on SEM images were the projected angle  $\theta$  of nano-pyramids. Yet, the angles measured by STEM along the zone axis of  $\langle 11-20 \rangle$  were the exactly basal angle  $\phi$  of nano-pyramid, as shown on figure 3-7b. The relation between the two angles is  $\phi = \tan^{-1}\{2 \cdot \sqrt{3} / \tan 2\}$ . The STEM-measured angles of  $74.16$  degrees compared with the theoretical value of  $74.88$  between the  $\{20-21\}$  and  $(0001)$  planes further demonstrates that the pyramidal plane of the nano-pyramids is the  $\{20-21\}$  plane. Figure 3-7c shows the schematic model of the nano-pyramid with the relevant planes identified.

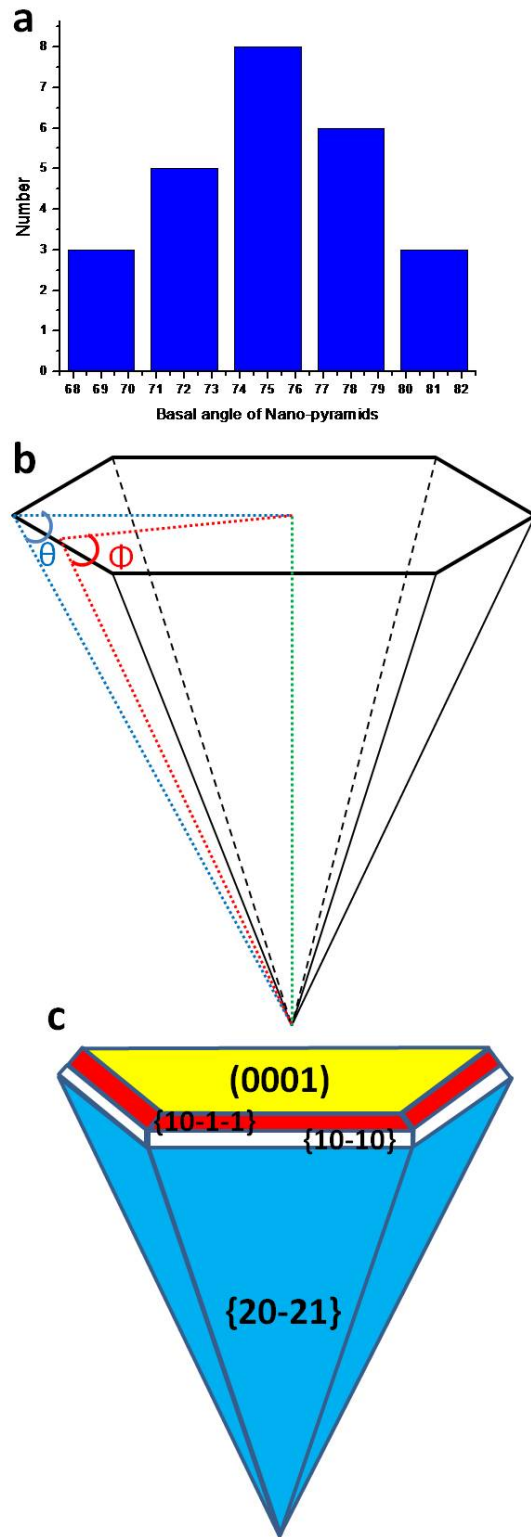


Figure 3-7: (a) Histogram of basal angle of nano-pyramid measured by STEM images; (b) Geometrical illustration of basal angle and projected angle of nano-pyramid; (c) Schematic illustration of individual nano-pyramid.

Therefore, all surfaces for the nano-pyramid decorated microwire are indentified. Based on the facets of the as-grown microwires, the surface area ratio of polar {0001}, polar {10-11} and non-polar {10-10} are 34.40%, 32.80% and 32.80%, respectively. The total polar surface occupies approximately 70% of the total surfaces. In addition, the as-grown nanostructures have atomic clean surfaces revealed by the STEM images, suggesting that the modulated pyramidal surfaces are stable in the air environment.

### **3.1.3. Possible growth mechanism of nano-pyramid decorated microwires**

Based on the SEM observation of the as-grown product, it is believed that the nano-pyramids grew on the primary ZnO prisms. Thus the growth process of the nano-pyramids may be due to a secondary nucleation<sup>13</sup>, and the stability of the pyramidal planes is probably due to minimization of surface energy<sup>35 36</sup>. The secondary growth was probably induced on the surface defect as nucleation sites, such as stacking faults<sup>37</sup>. The detailed growth process of nano-pyramids and the secondary growth mechanism were still not clear, but an interesting observation of decoration position was interesting, which may imply the growth of nano-pyramids. Almost all nano-pyramid decorated wires were found on the top layer of materials on the substrate. In the base region, no pyramid decorated structures were found. Some standing-up wires with continuous surface modifications showed it more clearly, as shown in figure 3-8. Figure 3-8(a) is a low magnification SEM image that shows a microwire standing up on the substrate. Detailed examination of this wire at different positions reveals that their surface patterns are changed (labeled in 3-8a), as shown in the figures 3-8 b-e. At the lower region of the wire near the base, it clearly shows its prism surfaces are smooth. Looking upward along this wire reveals the surface patterns began to be modified. When it reaches a specific height, the prism of wire was covered by pyramidal pattern fully. This

observation was in agreement with the distribution of nano-pyramid decorated nanostructures, which were more developed on the top layer of materials.

The reason for the presence and induction time of the surface etching is still not clear, but possibly the induction happened at the end of the synthesis process. The nanostructures on the top tend to have this pyramid decorated patterns since the structures on the top had more chance to contact the growth species ( $Zn^{2+}$  and  $O^{2-}$ ) to nucleate.

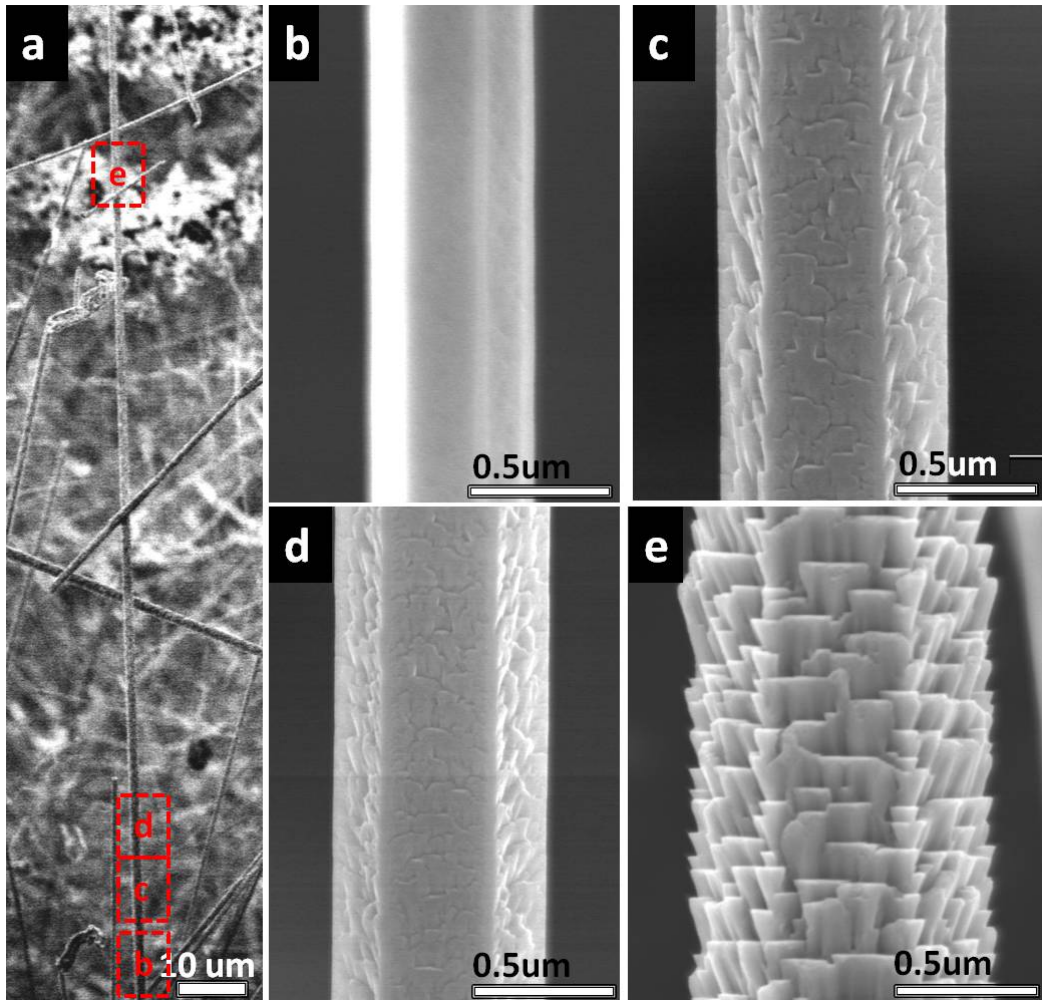


Figure 3-8: SEM images of different decoration pattern depending on different nanowire's diameters: (a) Low magnification microwire with diameter change (b) Non decoration pattern on the small diameter nanowire; (c) Surface step decoration pattern of nanowire; (d) Small nanopyramid decoration pattern of nanowire; (e) nanopyramid decoration pattern of nanowire.

STEM observation of as-grown ZnO nano-pyramids decorated on prism surfaces of ZnO microwires reveals that the as-grown microwires have atomic clean surfaces, which indicates that both pyramidal planes and atomically flat basal planes are quite stable in the air environment. The combination of polar {10-11} facets and non-polar {10-10} facets to form ZnO {20-21} planes plays a significant role for the stability of nanowire surfaces. The stability of ZnO {20-21} planes could be explained by crystalline kinetics, which is widely investigated in the field of surface science and solid state physics.

## **3.2. Spontaneous surface ordering of ZnO Nanostructures by Physical Vapor Deposition**

### **3.2.1. Synthesis of grooved surface ZnO nanowires**

The as-grown nanostructures were synthesized in a high temperature horizontal tube furnace by a standard evaporation-condensation process (PVD). Three grams of source materials (carbon black mixed zinc oxide powders at weight ratio at 1:2) was put in an alumina combustion boat placed in the center of a horizontal tube furnace. Ceramic substrates were placed downstream for collecting the growth product. The inner tube was refilled by oxygen mixed argon as carrier gas. The flow rate of argon and oxygen are 40 sccm and 15 sccm, respectively. The source materials were heated to 1000°C for two hours. No pumping system applied during the process. The grooved nanowires were collected on the ceramic substrates at the temperature region between 700°C and 800 °C. The grooved tetrapods were collected on the ceramic combustion boat in the middle of the tube.

### **3.2.2. Characterization of grooved surface ZnO nanowires**

Grooved nanowires can be synthesized by using oxygen-argon mixed gas at the ratio of 1:2 as carrier gas. Detailed synthesis method can be found at the method part in this

chapter. The as-grown groove surfaced nanowires were examined by Field-emission Scanning Electron Microscope (FE-SEM), as shown in figure 3-9.

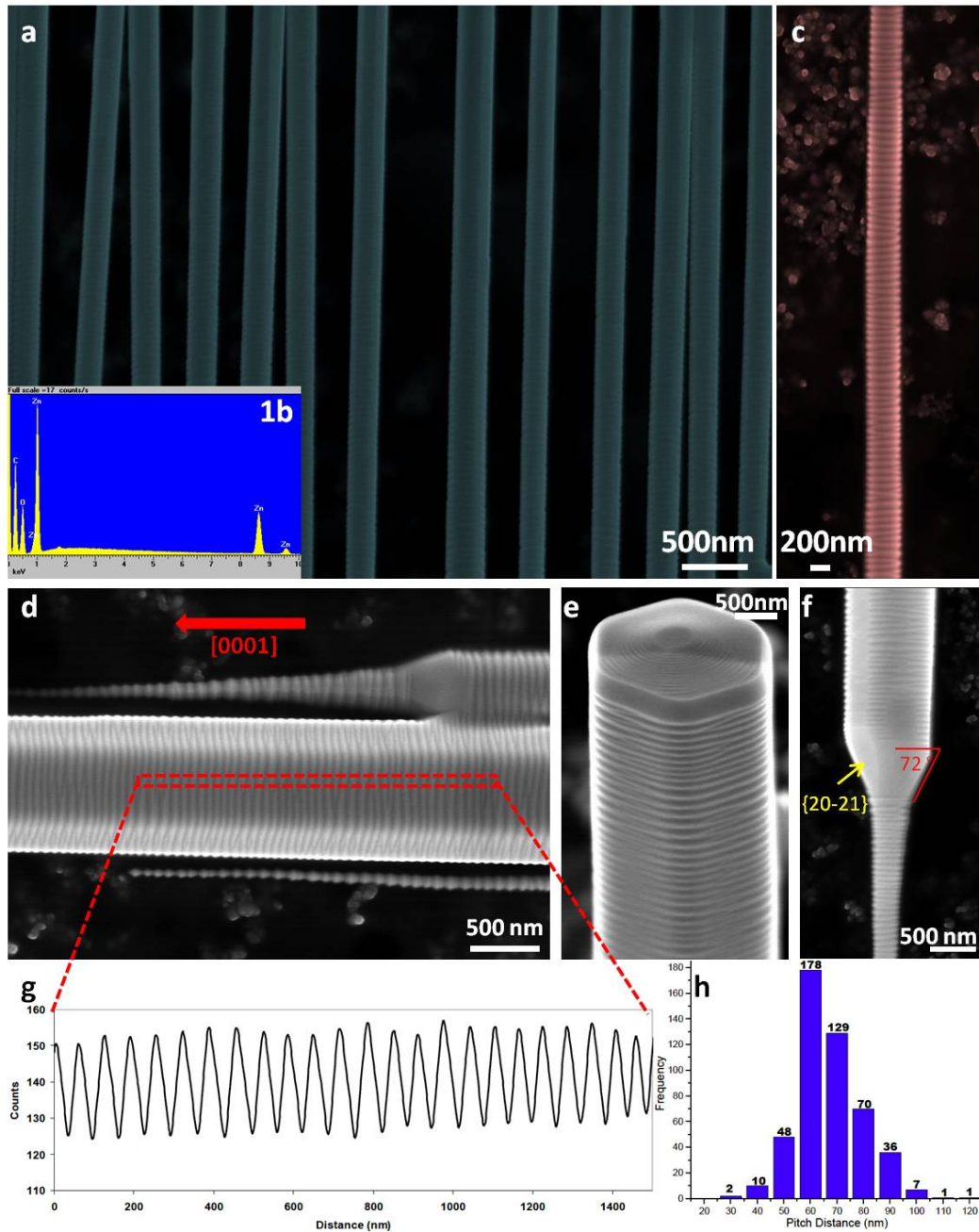


Figure 3-9: SEM images of as-grown nanostructures: (a) low magnification SEM image of as-grown nanostructures; (b) X-ray energy dispersive spectroscopy of as-grown nanowires; (c-f) High magnification SEM image of as-grown nanostructures, showing the extremely uniform decoration of surface grooves on the nanowires prism surfaces; (g) Intensity line profile across the surface grooves on a nanowire shows the quasi-periodic nature of the grooves with an average pitch distance of 62 nm; (h) Histogram of 483

pitch distances measured from many nanowires of various diameters. (thank Dr. J. Liu for taking the HR-SEM images)

Figure 3-9a shows a medium magnification SEM image revealing many nanowires with rough prism surfaces. The X-ray energy dispersive spectroscopy (EDS) of as-grown nanowires was performed as shown in figure 3-9b, which indicated the component of as-grown grooved nanowires is ZnO. Many nanowires with grooved surfaces were characterized by SEM, and two major types of nanowires were found. The first type nanowire has round prism, and the second type nanowire has hexagonal prism. Figure 3-9c is a high-resolution SEM image shows the first type nanowires. It is clear to see the presence of surface corrugation or grooves on the nanowires. By examining many round grooved nanowires, it was found that the diameter of those was usually between 30 nm and 300 nm. Figure 1d and 1e are high-resolution SEM images shows the second type nanowires. On figure 3-9d, it is clear to see that this type of nanowires have hexagonal prism as cross-section. By examining many as-grown nanowires of second type, it shows those nanowires has smallest diameter at 800 nm, and their diameter can be increased up to 2  $\mu\text{m}$ . Based on previous experiences, the growth direction of both two types of nanowires should be the ZnO (0001) direction. Another interesting observation is that, no nanowires have diameter between 300 nm and 800 nm were found. For many hexagonal nanowires, they usually have a pyramid-like transition region, as shown in figure 3-9f. In addition, those pyramid-like transition regions always continue to become rounded nanowires. This phenomenon may suggest that the grooved pattern may not be stable on the nanowires between 300 nm and 800 nm in diameter, or the stability of those grooved pattern may be depend on certain diameter, which is referring to certain surface energy. By analysis of many pyramid-like transition regions of grooved

nanowires, we estimated the average basal angle of the pyramid region is about  $72^\circ$ , which suggests that the pyramidal surface is made up by the ZnO {20-21} planes, in agreement with our previous work. Figure 3-9g is an intensity profile across the grooves on the nanowire in figure 1d, showing the quasi-periodic nature of the surface grooves with an average pitch distance of 62 nm. In order to know the pitch distances of the grooves of the whole sample, we performed measurements of the pitch distances on many nanowires. Figure 3-9g shows the histogram of 483 measurements. The mean value of the pitches was measured to be 62 nm, and the standard deviation is about 12 nm. The tip regions of nanowires have size below about 100 nm in diameter and the average pitch distances are larger, about 74 nm. Since the surface grooves are perpendicular to the growth (0001) direction of nanowires, so we named this type of surface groove as (0001) induced surface grooves.

### **3.2.3. Thermodynamic model for the periodic distance's dependence on nanowires' diameters**

(0001) induced surface grooved pattern is most common one on ZnO nanowires. By lots of characterization, it is believed that the grooved surface facet period depended on the diameter nanowires. A thermodynamic model for the facet period on nanowires was reported recently<sup>38</sup>, and can be used to explain the dependence of grooved period on nanowires' diameters.

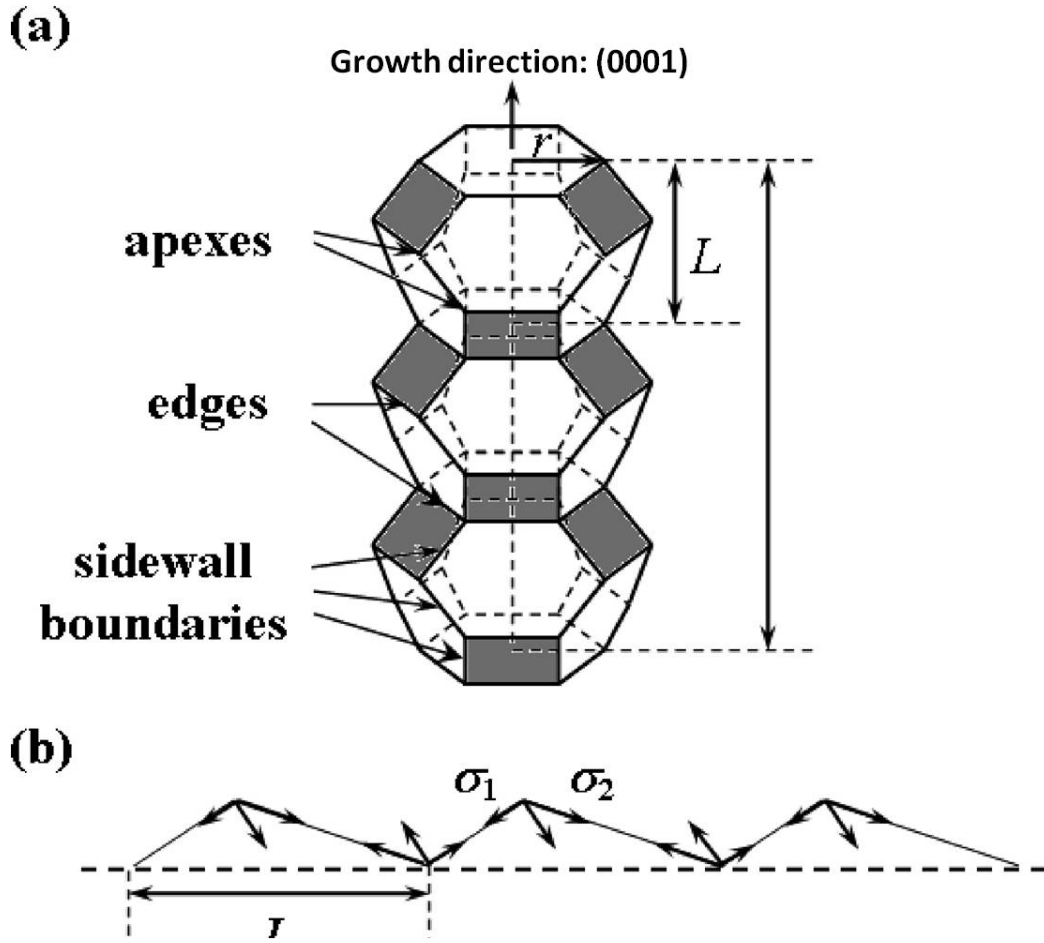


Figure 3-10 (a) schematic diagram of the three-dimensional grooved structure; (b) schematic diagram of the two-dimensional periodic faceting on the ZnO nanowires' sidewall surfaces. (The schematic diagrams are from the literature<sup>33</sup>)

In this model, following variables were defined as below. The wire's diameter is assumed as  $2r$ , and the cross-section is a regular hexagon before faceting occurs. The total free energy  $f$  of the faceted nanowire sidewall per unit projected area is given by<sup>39</sup>:

$$f = f_{\text{surf}} + E_{\text{boundaries}} + E_{\text{elastic}} \quad (1)$$

Finally, the expression for the free energy of the faceted nanowire surface per unit projected area was deduced into<sup>33</sup>:

$$f = (c_1 \gamma_{\{10-10\}}^0 + c_1 \gamma_{\{10-11\}}^0) + \left[ 2 \frac{\eta}{L} + 2 \frac{B}{rL} + \left( \frac{2c_3 \eta_1 + c_4 \eta_2}{r} \right) \right] - \frac{g}{L} \ln \left( \frac{L}{b\pi} \right) \quad (2)$$

$f$  has a minimum when the period of faceting  $L$  is

$$L = b\pi \exp \left( 2\frac{\eta}{g} + 1 + \frac{4\beta}{g2r} \right) \quad (3)$$

From equation 3, only the term in the argument of the exponential that arises from the apex energy is dependent on wire diameter,  $2r$ . It indicates that the periodic facet distance increase with decreasing of diameter, and decrease with increasing of diameter, which is in agreement with our SEM characterization.

### 3.2.4. Growth mechanism of grooved surface nanowires

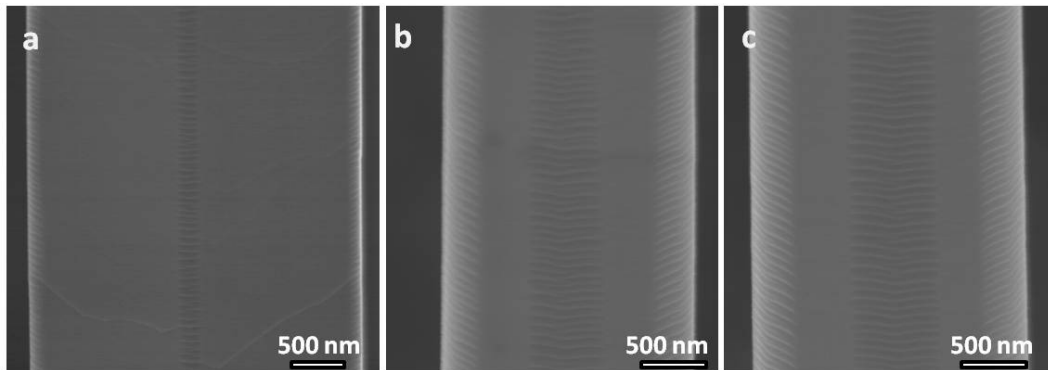


Figure 3-11: SEM images of different surface grooved pattern in different regions in diameter: (a) surface grooved pattern began to grow at the edges of nanowires; (b-c) surface grooved pattern trend to expand to cover the whole nanowire.

Based on large amount of SEM observation of as-grown grooved nanowires, we observed that for some nanowires, it has different morphology at different regions of different diameter. Those morphologies or surface patterns are different, but should be correlated, as shown in figure 3-11, which may reveal that the trend of surface pattern formation of grooved nanowires. Figure 3-11 are three SEM images shows surface patterns at different regions of the same nanowire. It seems like that the smooth surface nanowires were grown firstly, and the grooves grown on the wire's prism latterly. More importantly, the grooved pattern seems to grow at the corners of wire prisms, and then expand outward in order to enclose the whole prism. The grooves started at the corners, probably due to the fact that the corners are high-energy sites.

The surface ordering is again may be related to the theory of the secondary nucleation. The formation of the ordering of the grooved structures may be related to minimizing the total surface energy under specific growth environment<sup>9</sup>. The overall surface ordering of surface grooves can be described as following: Initially, the ZnO grows along [0001] direction to form hexagonal prism nanowires. Later on, the deposition of ZnO at the prism edges of nanowires resulted in ordered facets in order to reduce the stress and minimize the energy there.

### **3.2.5. Characterization of other surface grooved patterns**

#### ***3.2.5.1. Characterization of <11-20> induced surface grooved pattern on ZnO microwires***

In addition to the (0001) induced surface pattern discussed above, there is another surface pattern observed in the as-grown sample, as shown in figure 3-12. Figure 3-12a is a low magnification SEM image showing a very long nanowire, about 500  $\mu\text{m}$ . The medium magnification SEM image of figure 3-12b revealing the surface grooves were covered in the whole nanowire, which are parallel with nanowire's (0001) growth direction. Figure 3-12c and 3-12d are high magnification SEM images, revealing the edge of nanowire, and the top-view or prism surface of nanowire. The island at the prism edge of nanowire look like the induced site of surface pattern, which may grow along the ZnO {11-20} direction. Since the surface grooves are perpendicular to the ZnO {11-20} directions, we named this type of surface pattern as {11-20} induced surface grooves.

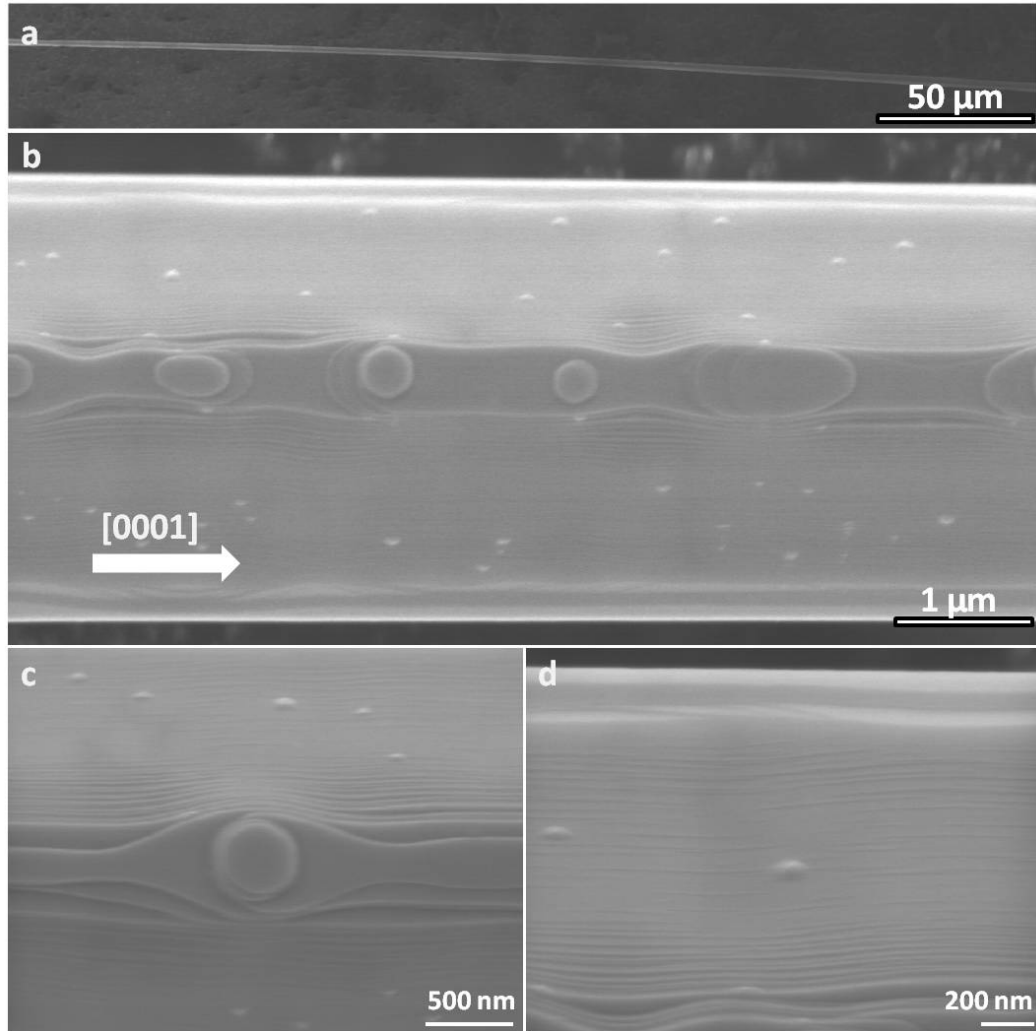


Figure 3-12: SEM images of  $\{11-20\}$  induced surface grooves on nanowires: (a) Low magnification microwire; (b) Medium magnification SEM image shows the surface grooves on the nanowires; (c) High magnification SEM image of edge of nanowire; (d) High magnification SEM image of nanowire's top-view.

### 3.2.5.2. Characterization of grooved surface patterns on ZnO micro tetra-pods

The grooved surface pattern was not only found on nanowires, but also found on other structures, like micrometer scale tetrapods, as shown in figure 3-13. Figure 3-13a and b are two high resolution SEM images showing two tetrapods structures, have (0001) induced and  $\langle 11-20 \rangle$  induced surface grooves, respectively.

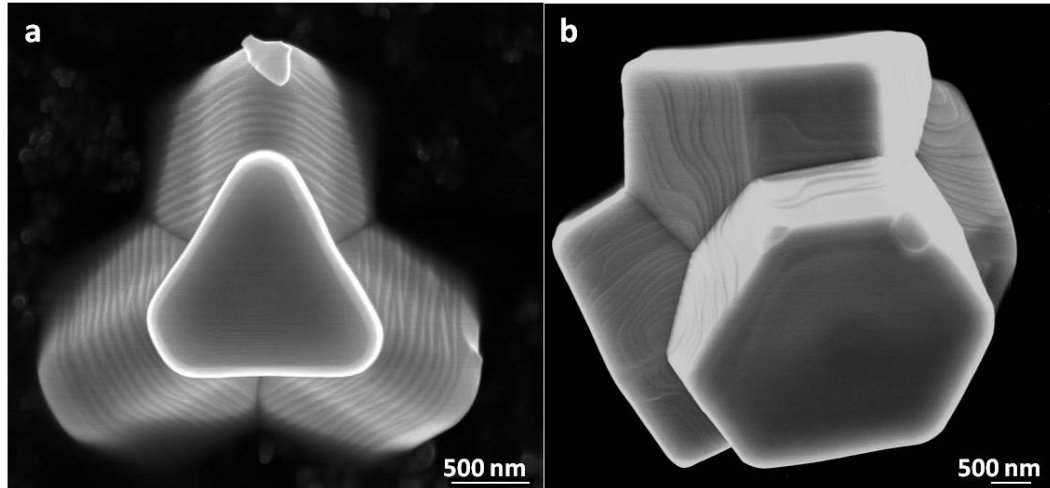


Figure 3-13: SEM images of surface grooved tetrapods: (a) High magnification SEM of tetrapod shows the (0001) induced surface grooves; (thank Dr. J. Liu for taking the HR-SEM images) (b) High magnification SEM of tetrapod shows the {11-20} induced surface grooves.

#### ***3.2.5.4. Synthesis and characterization of surface grooved pattern on ZnO microbelts***

The as-grown nanostructures were synthesized in a high temperature horizontal tube furnace by a standard evaporation-condensation process (physical vapor deposition). 3 grams source materials (carbon black mixed zinc oxide powders at weight ratio at 1:2) were putted in an alumina combustion boat placed in the center of a horizontal tube furnace. Ceramic substrates were placed downstream for collecting the growth product. The inner tube was refilled by oxygen mixed argon as carrier gas. The flow rate of argon and oxygen are 60 sccm and 21.5 sccm, respectively. The source materials were heated to 1000°C for two hours. No pumping system applied during the process. The grooved microbelts were collected on the ceramic substrates at the temperature region between 700°C and 800 °C.

For the belt-like structure, they also have a surface groove pattern, although, its details is not similar with nanowires' and tetrapods', as shown in figure 3-14. Figure 3-

14a is a low magnification SEM image showing a belt-like structure. For ZnO belt structures, their growth direction are usually (0001) or {11-20} direction. Figure 3-14b-d are high resolution SEM images revealing the details of the surface grooves. The corrugations are neither parallel with nor perpendicular to the growth direction of belt structure. At different region of this nanowire, we find the surface pattern was changed as shown in figure 3-14f-h. We can observe that there were other surface grooves perpendicular to the initial grooves, which showed up in some region, and competed with the dominant surface grooves. The final surface pattern, as shown in figure 3-14g and 3-14h, was a combination of the two surface grooves. The formation mechanism for this surface pattern is not clear. Further study on it will be performed in the near future.

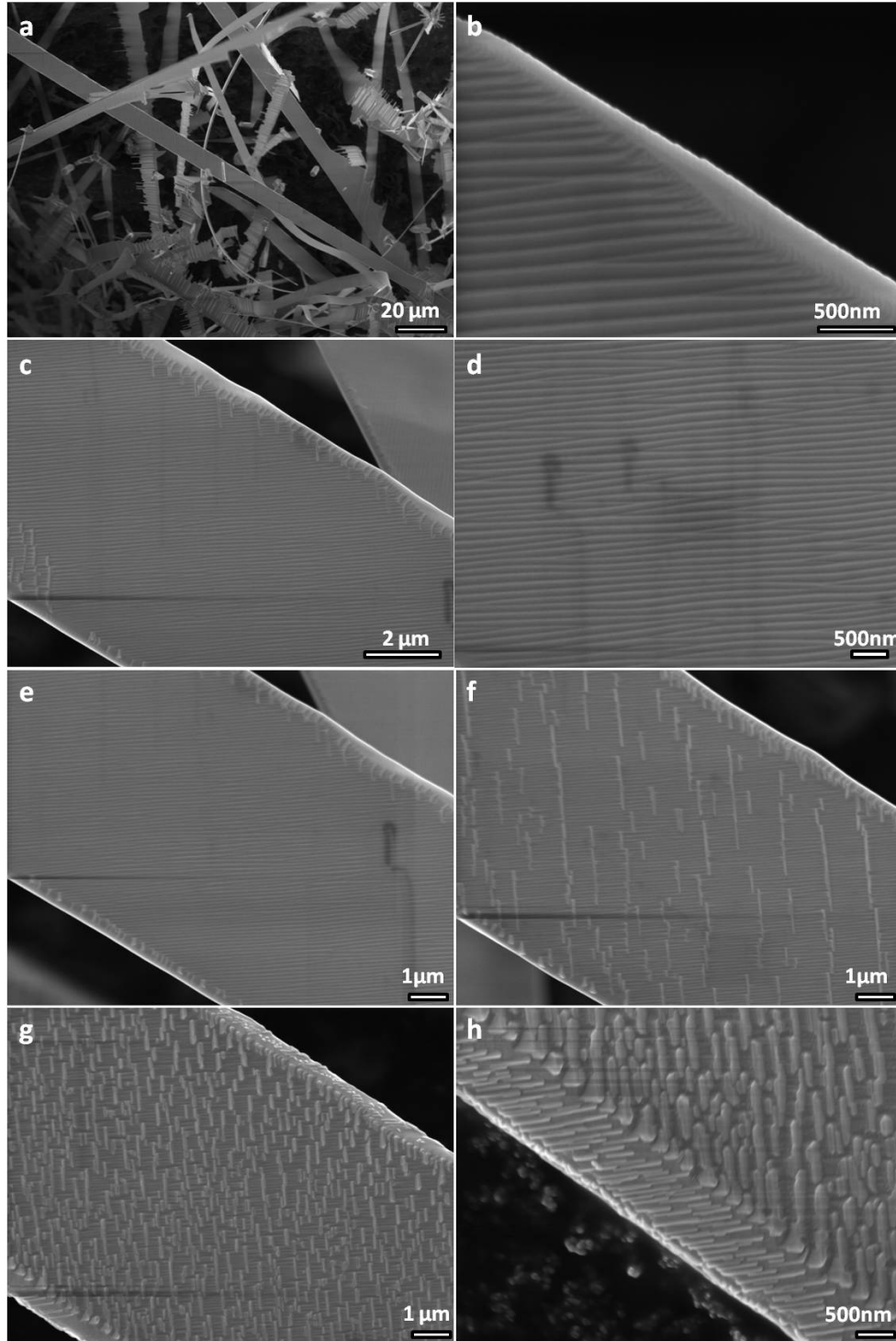


Figure 3-14: SEM images of surface grooved belt-like structure: (a) Low magnification microbelt with surface grooves; (b) High resolution SEM image of belt shows the edge of belt; (c-e) High resolution SEM image shows the surface grooves on the belt; (f) another type of surface grooves began to introduced on the surface; (g) High resolution SEM of the two dimensional surface grooved pattern; (h) High resolution SEM of the edge of belt, showing the surface grooves there.

## **Chapter 4: The Effects of Oxygen Partial Pressure on the Morphologies of ZnO Nanostructures and their high yield synthesis**

### **4.1. High-yield synthesis of characterization of several typical nanomaterials due to the effect of oxygen partial pressure**

Our recent synthesis work reflects that the oxygen partial pressure was one of very important parameters affecting the components and morphologies of nanostructures. This effect of oxygen partial pressure is critical for ZnO nanomaterials' synthesis by using our PVD system with silicon seal stoppers. In our PVD system, the seal stoppers were changed from Teflon one to silicon one, in order to seal the tubes better. Details about seal stoppers system was introduced in the degree thesis of previous member in our group<sup>40</sup>. After this change, we found the results of nanostructures growth were significant different by two different seal stoppers, although the same growth conditions were performed. By using the old seal stoppers (Teflon stoppers), ZnO nanostructures can be grown by using pure argon or nitrogen as carrier gas. However, by using the new stoppers sealing the tubes (silicon one), only Zn nanostructures can be grown by pure argon/nitrogen as carrier gas. ZnO nanostructures can be grown only if proper amount of oxygen mixed with argon or nitrogen, and used together as carrier gas. This phenomenon indicates that, in our system, the growth of ZnO nanostructures needs enough oxygen partial pressure in order to nucleate to ZnO nanostructures. The reasons are that, silicon stoppers can seal the tube better to inhibit the oxygen leaking into the tube, which leads a lower oxygen pressure. However, Teflon stoppers cannot seal the tube very well, so oxygen leaking into the tubes promotes a higher oxygen partial pressure. More important, under this oxygen-mixed synthesis environment, ZnO nanostructures showed novel macroscopic morphologies, such as gel-like and form-like

macroscopic morphologies, which were quite different with the general wool-like morphology of ZnO nanostructures. In addition, it was found that by increasing the amount of carrier gas during the nanomaterials' synthesis process, the yield of nanostructures can be improved.

In this chapter, several typical nanostructures novel macroscopic morphologies synthesized under the oxygen-mixed environment will be introduced.

#### **4.1.1. Zn microparticles**

##### ***4.1.1.1. Synthesis of Zn microparticles***

The as-grown nanostructures were synthesized in a high temperature horizontal tube furnace by a standard evaporation-condensation process (physical vapor deposition). Three grams of source material (carbon black mixed zinc oxide powders at weight ratio at 1:2) were put in an alumina combustion boat placed in the center of a horizontal tube furnace. Ceramic substrates were placed downstream for collecting the growth product. The inner tube was refilled by pure argon as carrier gas. The flow rate of the carrier is not important, but is likely in the range between 20 sccm up to 100 sccm. The source materials were heated to 1000°C for two hours.

##### ***4.1.1.2. Characterization of Zn microparticles***

By using pure argon or nitrogen as carrier gas, large amount of grey dust-like materials were collected after the synthesis process, as shown in the optical image (fig. 4-1a). Those grey as-grown materials were distributed at a large temperature region between 800°C through the region of room temperature, as shown in the optical image (fig. 4-1a). Scanning electron microscopy was used to examine the detailed as-grown materials. Figure 4-1b is a low magnification SEM image of as-grown materials. In this image, the grey dust-like as-grown materials contained micrometer scale particles. By

abundant examination of those as-grown materials, those particles have a range of diameter between 1  $\mu\text{m}$  and 10  $\mu\text{m}$ , as shown in the medium magnification SEM image (fig. 4-1d). High-resolution SEM image of typical particles (fig. 4-1e) reveals the presence of nano-facets on the surface of microparticles.

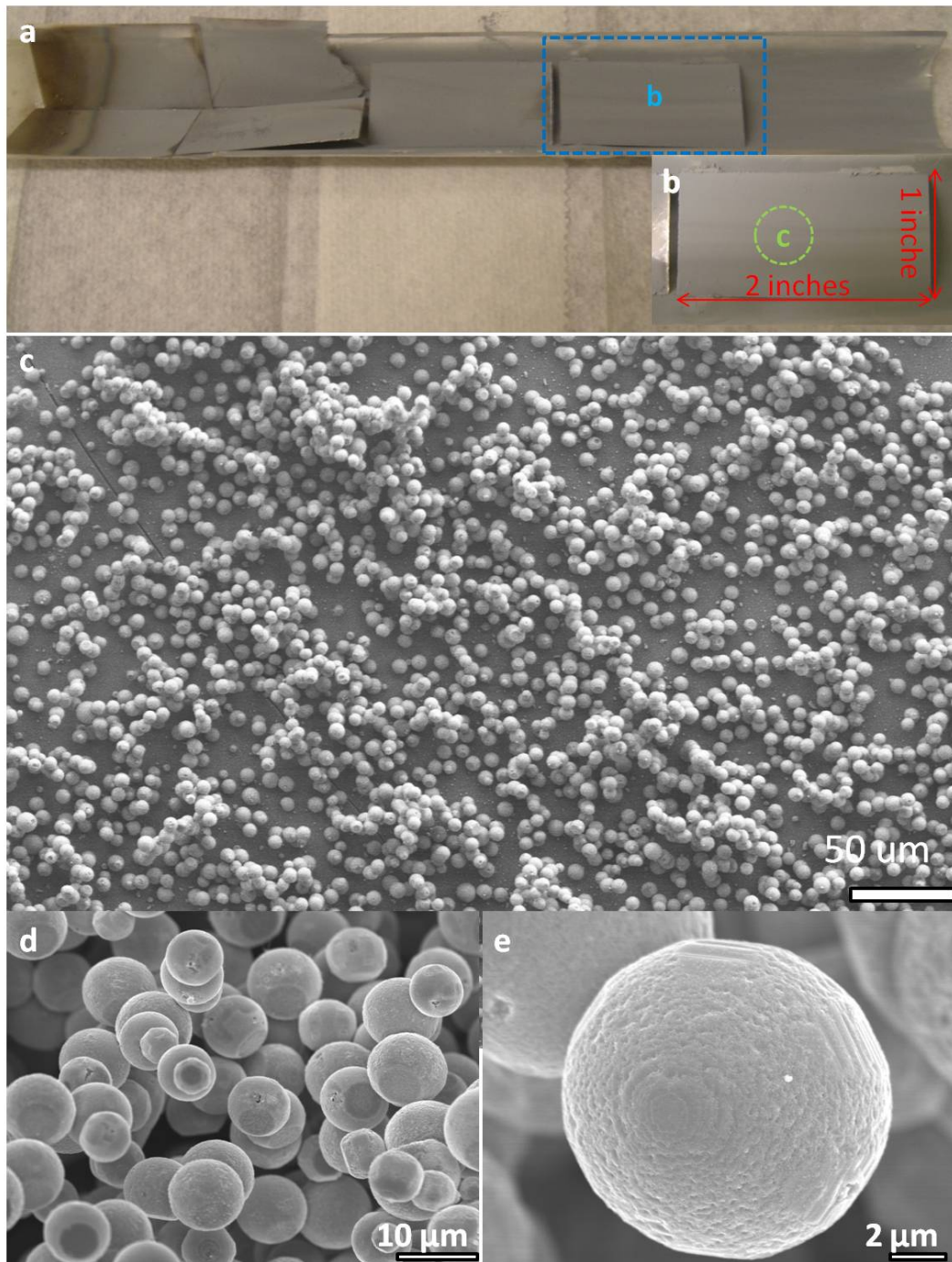


Figure 4-1: (a) optical image shows high yield materials synthesized by one run. (b) one piece of substrate selected shows the grey color dust like materials. (c) low magnification SEM image of grey dust-like materials, shows the micrometer scale particles. (d) medium magnification SEM image of microparticles reveals they have a range in diameter between 1  $\mu\text{m}$  and 10  $\mu\text{m}$ . (e) high-resolution SEM image of a typical microparticle shows clear surface facets.

The as-grown materials had been further examined by X-ray diffraction (XRD), which gave pure Zn structure, as shown in the figure 4-2.

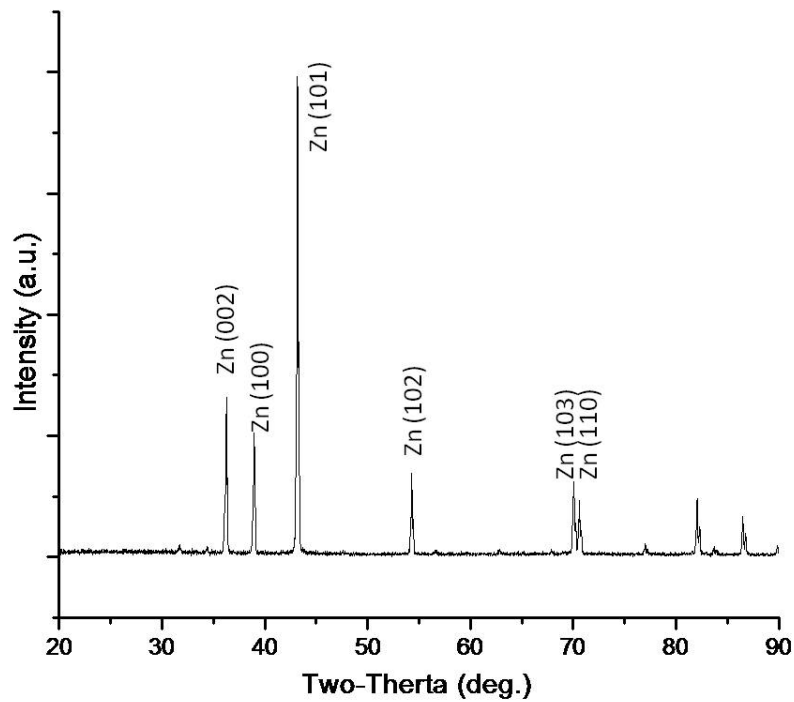


Figure 4-2: XRD spectrum of grey dusk-like materials shows Zn structure of as-grown materials.

Zn dust-like materials were duplicated many times under the oxygen-free environment. It may imply that ZnO structures cannot be grown if there were not enough oxygen vapors for the nucleated and grown process.

#### **4.1.2. Grey gel-like nanomaterials**

10-20% oxygen was mixed with argon as carrier gas in order to get ZnO nanostructures.

##### ***4.1.2.1. Synthesis of grey gel-like nanomaterials***

The as-grown nanostructures were synthesized in a high temperature horizontal tube furnace by a standard evaporation-condensation process (physical vapor deposition). 3 grams source materials (carbon black mixed zinc oxide powders at weight ratio at 1:2) were putted in an alumina combustion boat placed in the center of a horizontal tube furnace. Ceramic substrates were placed downstream for collecting the growth product. The inner tube was refilled by 10-20% oxygen mixed argon as carrier gas. The total flow rate of carrier is 55 sccm. The source materials were heated to 1000°C for two hours. As-grown gel-like materials were collected in the temperature region between 200°C to 400°C.

##### ***4.1.2.2. Synthesis of grey gel-like nanomaterials***

By the synthesis within 10-20% oxygen-mixed argon as carrier gas, the as-grown materials and their distribution was quite complicated. At the room temperature zoom near the tube's downstream end, lots of grey dust-like materials can be still obtained. By SEM characterization, the morphologies of those grey dust-like materials were also micrometer particles which were same to the particles mentioned above. However, at the temperature zoom between 200°C and 400°C, large amount of grey color gel-like materials were obtained, as shown in the optical image below (fig. 4-3a). Those as-grown materials were very soft and can be easily torn, which was never seen in any previous literature

Those gel-like as-grown materials were further examined by SEM. Figure 4-3b is a low magnification SEM image of as-grown grey gel-like materials. It seems that those gel-like

nanomaterials was made up of flower-like clusters. Figure 4-3c is a medium magnification SEM images indicates that the density of those flower-like cluster was very high, which may play an important role for the gel-like macroscopic morphology of as-grown nanomaterials. Figure 4-3d is a individual typical flower-like nanocluster. It is clear to see that the cluster has a core, and lots of nanowires are grown from the core.

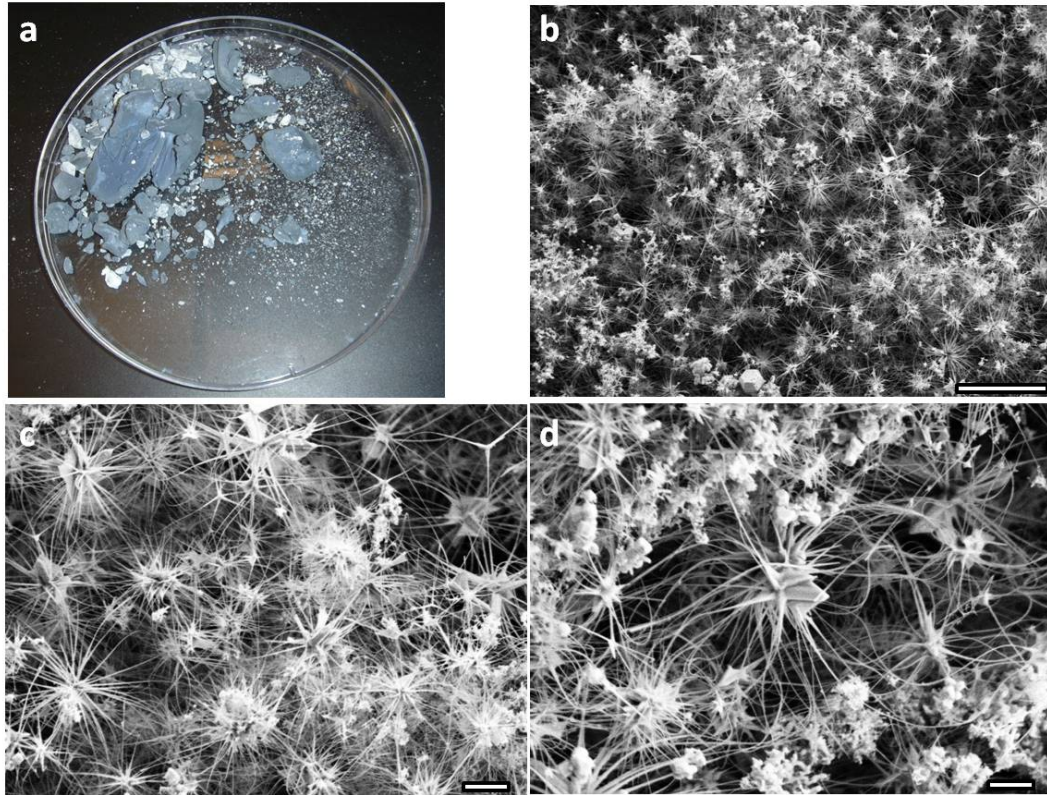
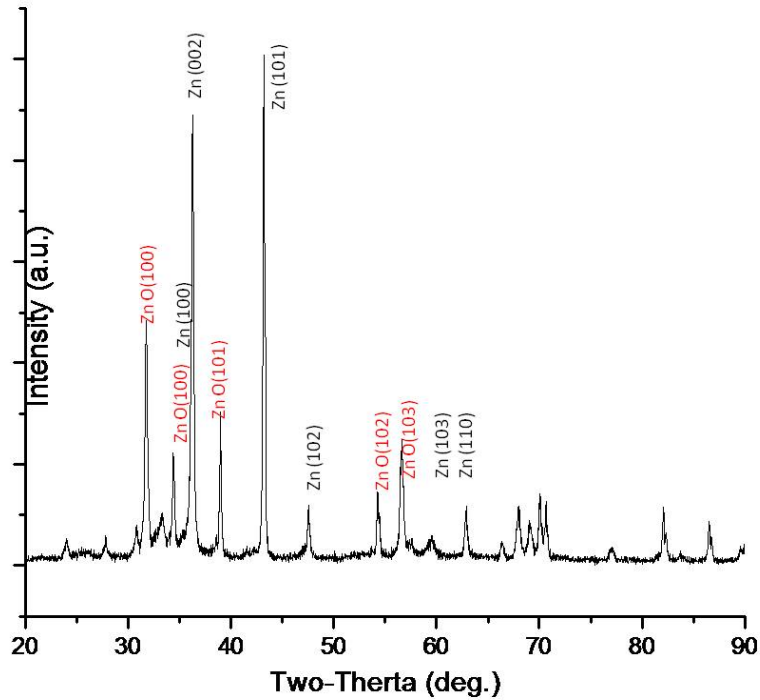


Figure 4-3: (a) optical image of grey gel-like materials. (b) low magnification SEM image of gel-like as-grown materials. (c) Medium magnification SEM image shows the cluster structures of gel-like materials. (d) High-resolution SEM image show a typical nanocluster.

The as-grown grey gel-like nanomaterials were examined by X-ray diffraction (XRD). XRD spectrum gave both ZnO wurtzite structure and Zn structure for as-grown grey gel-like materials, which implied the  $ZnO_x$  structure of the as-grown grey gel-like materials,

as shown in figure 4-4. The Zn component in the materials may contribute to the grey color of as-grown gel-like materials.



4-4: XRD spectrum of grey as-grown gel-like materials.

### 4.1.3. White gel-like ZnO nanomaterials

#### 4.1.3.1. Synthesis of white ZnO gel-like materials

The as-grown nanostructures were synthesized in a high temperature horizontal tube furnace by a standard evaporation-condensation process (physical vapor deposition). Three grams source materials (carbon black mixed zinc oxide powders at weight ratio at 1:2) were putted in an alumina combustion boat placed in the center of a horizontal tube furnace. Ceramic substrates were placed downstream for collecting the growth product. The inner tube was refilled by 20-30% oxygen mixed argon as carrier gas. The

total flow rate of carrier is 55 sccm. The source materials were heated to 1000°C for two hours. As-grown gel-like materials were collected in the temperature region between 200°C to 400°C.

#### ***4.1.3.2. Characterization of white ZnO gel-like materials and ZnO tree-like materials***

Figure 4-5a is an optical digital image of as-grown ZnO white gel-like materials. The gel-film is also very soft and lightweight and can be easily torn. These structures sometimes look like a film and sometimes look like paste. They usually grew in the lower temperature zone of the tube furnace with temperatures ranging from about 300°C to 400°C. Large-scale synthesis of such structures is possible. Figure 4-5b shows a SEM image of the as-grown gel, revealing the presence of nanowires and some multipods. Detailed examination of many SEM images showed that almost all the nanowires are connected with each other; some multipods were also observed as shown in the image. Figure 4-5c is a high magnification SEM image of a typical nanowire showing the morphology of the nanowire and the regularity of the change of its diameter. Detailed measurements of the diameters of the nanowires showed that there was a bimodal distribution of nanowire diameters with their average size of 3 nm and 123 nm, respectively. The clusters usually connect the nearby nanowires together tightly, which is central for the macroscopic gel-like morphology. Figure 4-5d is a high resolution SEM image of typical multipods.

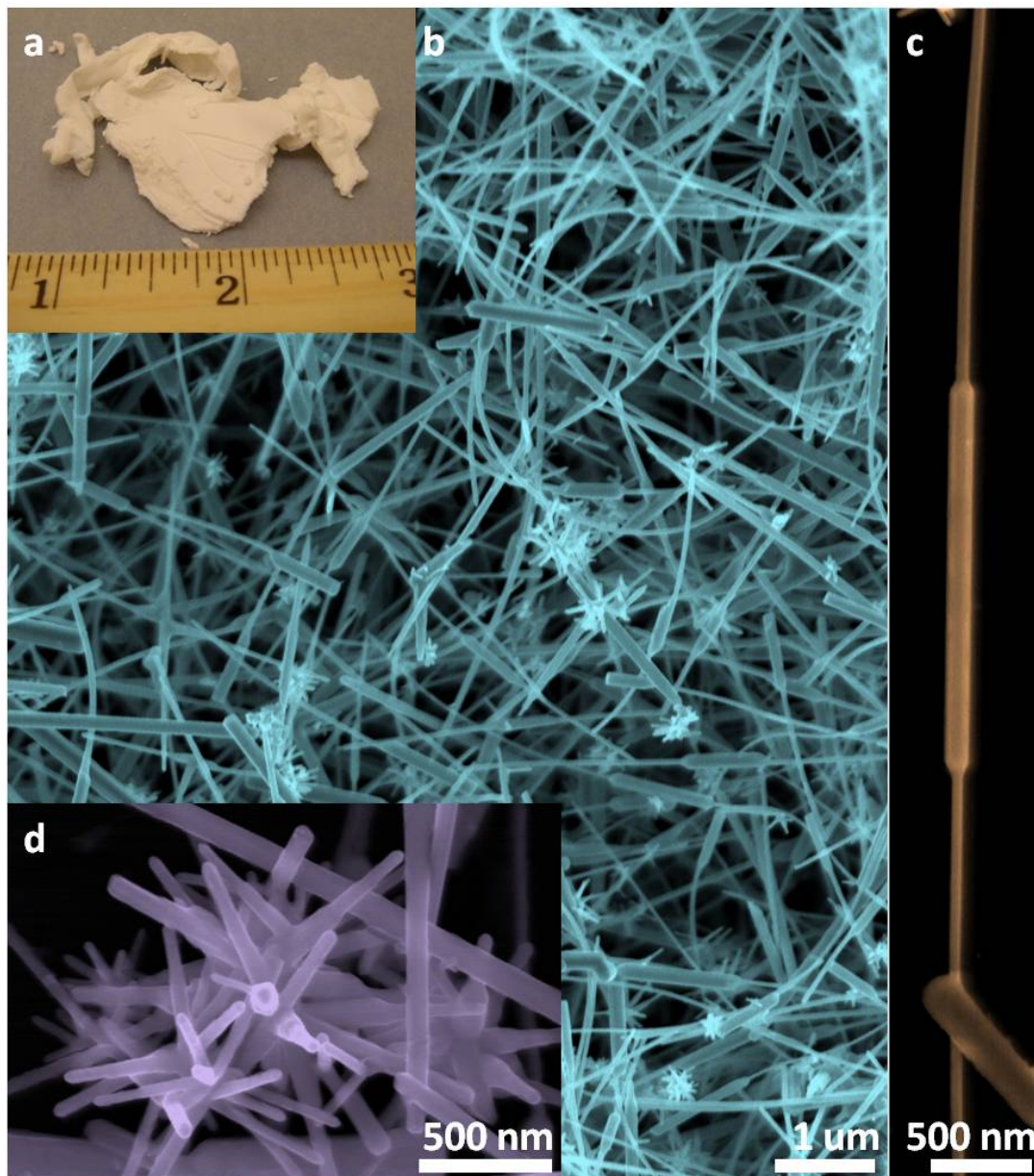


Figure 4-5: (a) optical digital image of as-grown nanomaterials showing the macroscopic soft gel-like morphology. (b) SEM image of as-grown ZnO soft gel revealing the interlacing and networked ZnO nanowires as well as some nanomultinods. (c) SEM image of a typical nanowire within the ZnO gel-like structure showing the bimodal distribution of the nanowire diameters and the joint of different nanowires. (d) SEM image of typical ZnO multipods.

The white gel-like materials were further examined by XRD, which reveals ZnO wurtzite structure of as-grown nanostructures, as shown in figure 4-6.

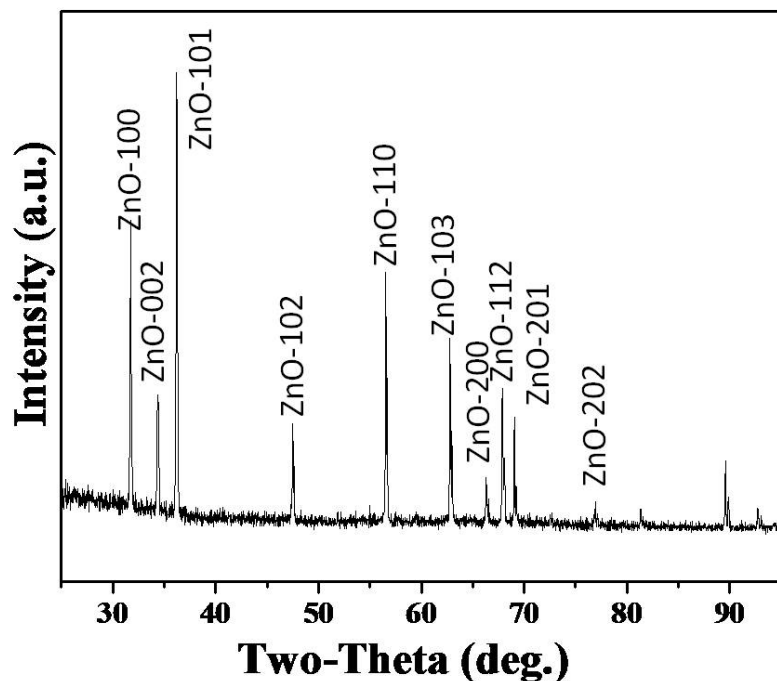


Figure 4-6: XRD spectrum of white as-grown gel-like materials.

#### 4.2. Reasons for large amount of as-grown products

For those as-grown materials mentioned above, their product amount is large. Usually, for every two grams of raw source material, the product weight is from 200 milligrams up to one gram. So this synthesis process has great potential for the high-yield synthesis, which is critical for being used widely for various applications in the industries. Based on abundant synthesis experience, we believed that the pumping-free synthesis environment had played an important role for the large amount of as-grown materials obtained in every synthesis circle. Since no pumping applied into our synthesis system, the carrier gas in the tube was expelled from the tube mechanically by the entrance of new carrier gas, which resulted super saturation of elemental vapor. Under this environment,  $Zn^{2+}$  cations and  $O^{2-}$  anions have a much higher possibility to meet and nucleate with the other to ZnO.

## APPENDIX: PUBLICATIONS

1. Dinghao Tang and Jingyue Liu, *Surface-grooved ZnO Nanowires and Tetrapods by Physical Vapor Deposition*, *Microscopy & Microanalysis*, **2010**, 16 (suppl. 2), 1264-1265.
2. Dinghao Tang, Hongyang Liu and Jingyue Liu, *Synthesis and Characterization of ZnO Nanostructures with Macroscopic Gel-like Morphology*, *Microscopy & Microanalysis*, **2010**, 16 (suppl. 2), 1286-1287.
3. Hongyang Liu, Dinghao Tang and Jingyue Liu, *Cold Catalyzed Growth of Three-dimensional Hierarchical ZnO Nanobelts*, *Microscopy & Microanalysis*, **2010**, 16 (suppl. 2), 1498-1499.
4. Dinghao Tang, Lawrence F. Allard and Jingyue Liu, *Nano-pyramid decorated ZnO Microwires by Vapor Phase Homo-epitaxial Growth*, **in preparation for submitting to ACS Nano**.
5. Dinghao Tang, Lawrence F. Allard and Jingyue Liu, *Synthesis and Characterization of Nano-pyramid Decorated ZnO Nanowires*, *Microscopy & Microanalysis*, **2009**, 15 (suppl. 2), 1154-1155.

## **VITA**

Dinghao Tang was born on January 8th, 1986 in Beijing, China. In July of 2008, he graduated from Peking University with a B.S. degree in Electronics, Beijing, China. In August of 2010, he received his M.S. degree in Physics from University of Missouri-St. Louis.

## REFERENCES

---

- <sup>1</sup> G.E. Moore. Cramming more componets onto integrated circuits, Proc. IEEE 1998, 86, 82. (Reprinted from Electronics, 114-117, April 19, 1965)
- <sup>2</sup> Peercy, P.S. The drive to miniaturization. **Nature**, 2000, 406, 1023.
- <sup>3</sup> Feynman, R. There's plenty of room at the bottom. Annual meeting of the American Physical Society, 1959.
- <sup>4</sup> Iijima, S. Helical microtubules of graphitic carbon. *Nature*, **1991**, 354(6348), 56-58.
- <sup>5</sup> Z.L. Wang (ed) Nanowires and nanobelts - materials, properties and devices, Vol. I: Metal and semiconductor nanowires, Kluwer Academic Publisher, **2003**.
- <sup>6</sup> C. R. Martin. Membrane-Based Synthesis of Nanomaterials, *Chem. Mater.*, **1996**, 8, 1739-1746.
- <sup>7</sup> Xia, Y.; Yang, P.; Sun, Y.; Wu, Y., Mayers, B.; Gates, B.; Yin, Y.; Kin, F.; Yan, H. One-Dimensional Nanostructures: Synthesis, Characterization, and Applications. *Adv. Mater.* **2003**, 15, 353-389.
- <sup>8</sup> M.H. Huang, S. Mao, H. Feick, H. Yan, Y. Wu, H. Kind, E. Weber, R. Russo, P. Yang, Room-Temperature Ultraviolet Nanowire Nanolasers, *Science*, **2001**, 292, 1897-1899.
- <sup>9</sup> Pan, Z.W.; Dai, Z.R.; Wang, Z.L. Nanobelts of Semiconducting Oxides. *Science*, **2001**, 291, 1947-1949.
- <sup>10</sup> Iijima, S. Helical microtubules of graphitic carbon. *Nature*, **1991**, 354(6348), 56-58.
- <sup>11</sup> Lu, W,; Lieber, C.M. Semiconductor nanowires. *J. Phys. D: Appl. Phys.* **2006**, 39, R387-R406.
- <sup>12</sup> Lu, J.; Chang, P.; Fan, Z. Quasi-one-dimensional metal oxide materials-Synthesis, properties and applications. *Mater. Sci. and Enge. R*, **2006**, 52, 49-91.
- <sup>13</sup> Wang, Z.L. Zinc oxide nanostructures: growth, properties and applications. *J. Phys.: Condens. Matter.*, **2004**, 16, R829-R858.
- <sup>14</sup> Huang, M. H.; Mao, S.; Feick, H.; Yan, H.; Wu, Y.; Kind, H.; Weber, E.; Russo, R.; Yang, P. Room-Temperature Ultraviolet Nanowire Nanolasers. *Science*, **2001**, 8, 1897–1899.
- <sup>15</sup> Gudixsen, M. S.; Lauhon, L. J.; Wang, J.; Smith, D. C.; Lieber, C. M. Growth of nanowire superlattice structures for nanoscale photonics and electronics. *Nature*, **2002**, 415, 617–620.

- 
- <sup>16</sup> Wang, Z. L.; Song, J. Piezoelectric Nanogenerators Based on Zinc Oxide Nanowire Arrays. *Science* **2006**, *312*, 242-246.
- <sup>17</sup> Li, Z.; Yang, R.S.; Yu, M.; Bai, F.; Li, C.; Wang, Z.L. Cellular Level Biocompatibility and Biosafety of ZnO Nanowires. *J. Phys. Chem. C*, **2009**, *112*, 20114-20117.
- <sup>18</sup> Wagner, R.S.; Ellis, W.C. Vapor-Liquid-Solid Mechanism of single crystal growth, *Applied Physics Letters*, **1964**, *4* (5), 89-90.
- <sup>19</sup> Wagner, R.S.; Ellis, W.C.; Arnold, S.M.; Jackson, K.A. *J. Appl. Phys.* **1964**, *35*, 2993
- <sup>20</sup> Dick, K.A.; Deppert, K.; Karlsson, L.S.; Wallenberg, L.R.; Samuelson, L.; Seifert, W. A New Understanding of Au-Assisted Growth of III-V Semiconductor Nanowires. *Advanced Functional Materials*, **2005**, *15*(10), 1603-1610.
- <sup>21</sup> Kong, X. Y.; Ding, Y.; Yang, R.; Wang, Z. L. Single-Crystal Nanorings Formed by Epitaxial Self-Coiling of Polar Nanobelts. *Science* **2004**, *303*, 1348–1351.
- <sup>22</sup> Gao, P. X.; Ding, Y.; Mai, W.; Hughes, W. L.; Lao, C. S.; Wang, Z. L. Conversion of zinc oxide nanobelts into superlattice-structured nanohelices. *Science*, **2005**, *309*, 1700–1704.
- <sup>23</sup> Lao, J. Y.; Wen, J. G.; and Ren, Z. F. Hierarchical ZnO Nanostructures. *Nano Lett.*, **2002**, *2*, 1287-1291.
- <sup>24</sup> Sounart, T. L.; Liu, J.; Voigt, J. A.; Huo, M.; Spoerke, E. D.; McKenzie, B. Secondary Nucleation and Growth of ZnO. *J. Am. Chem. Soc.*, **2007**, *129*, 15786-15793.
- <sup>25</sup> Zhang, T.; Dong, W.; Keeter-Brewer, M.; Konar, S.; Njabon, R. N.; Tian, Z. R. Site-Specific Nucleation and Growth Kinetics in Hierarchical Nanosyntheses of Branched ZnO Crystallites. *J. Am. Chem. Soc.*, **2006**, *128*, 10960-10968.
- <sup>26</sup> Sounart, T.; Liu, J.; Voigt, J.; Hsu, J.; Spoerke, E.; Tian, Z.; Jiang, Y. Sequential Nucleation and Growth of Complex Nanostructured Films. *Adv. Funct. Mater.*, **2006**, *16*, 335-344.
- <sup>27</sup> Eshelby, J.D. Screw Dislocations in Thin Rods. *J. Appl. Phys.*, **1953**, *24*, 176-179.
- <sup>28</sup> Bierman, M. J.; Lau, Y. K. A.; Kvit, A. V.; Schmitt, A. L.; Jin, S. Dislocation-Driven Nanowire Growth and Eshelby Twist. *Science*, **2008**, *320*, 1060-1063.
- <sup>29</sup> Zhu, J.; Peng, H. L.; Marshall, A. F.; Barnett, D. M.; Nix, W. D.; Cui, Y. Formation of chiral branched nanowires by the Eshelby Twist. *Nature Nanotech.*, **2008**, *3*, 477-481.
- <sup>30</sup> [https://wiki.umsl.edu/index.php/Talk:Reciprocal\\_Lattice](https://wiki.umsl.edu/index.php/Talk:Reciprocal_Lattice)

- 
- <sup>31</sup> Wanekaya, A.K.; Chen, W., Myung, N.V., Mulchandani, A. Nanowire-Based Electrochemical Biosensors, *Eleetroanalysis*, **2006**, 18, 533-550.
- <sup>32</sup> Daniel, S., Rao, T.P., Rao, K.S., Rani, S.U., Naidu, C.R.K., Lee, H.Y., Kawai, T. A Review of DNA Functionalized/Grafted Carbon Nanotubes and their Applications, *Sensors and Actuators B*, **2007**, 122, 672-682.
- <sup>33</sup> Katz, E., Willner, I. Biomolecule-Functionalized Carbon Nanotubes: Applications in Nanobioelectronics, *Chem. Phys. Chem.*, **2004**, 5, 1084-1104.
- <sup>34</sup> Li, Z.; Yang, R.S.; Yu, M.; Bai, F.; Li, C.; Wang, Z.L. Cellular Level Biocompatibility and Biosafety of ZnO Nanowires. *J. Phys. Chem. C*, **2009**, 112, 20114-20117.
- <sup>35</sup> Herring, C. *In Structure and Properties of Solid Surfaces*; Gromer, R, Smith, C. S., Eds.; University of Chicago: Chicago, 1953.
- <sup>36</sup> Mullins, W. W. *In Metal surfaces: structure, energetics, and kinetics*; American Society for Metals: Metals Park, OH, 1962.
- <sup>37</sup> Glushenkov, A. M.; Zhang, H.; Zou, J.; Lu, G. Q.; Chen, Y. Unusual corrugated nanowires of zinc oxide. *J. Crys. Grow.* **2008**, 310, 3139-3143.
- <sup>38</sup> Li, P.; Nellist, P.; Lang, C.; Cockayne, J. Dependence of surface facet period on the diameter of nanowires. *ACS Nano*, **2010**, 4(2), 632-636.
- <sup>39</sup> Shchukin, V, A.; Bimberg, D. Spontaneous ordering of nanostructures on crystal surface. *Rev. Mod. Phys.* **1999**, 71, 1125-1171.
- <sup>40</sup> Liu, S.; Synthesis and characterization of ZnO nanostructures, M.S. thesis submitted to Univ. MO - St. L, 2009 (August). (QC 176.8.N35.L58)